Fall 12-1-2022

AN INTEGRATED ELECTRONIC-SKIN PATCH FOR REAL-TIME AND CONTINUOUS MONITORING OF A PANEL OF BIOMARKERS COMBINED WITH DRUG DELIVERY

Tanzila Noushin
University of Texas at Tyler

AN INTEGRATED ELECTRONIC-SKIN PATCH FOR REAL-TIME AND CONTINUOUS MONITORING OF A PANEL OF BIOMARKERS COMBINED WITH DRUG DELIVERY

by

TANZILA NOUSHIN

A thesis submitted in partial fulfillment of the
requirements for the degree of

Master of Science in Electrical Engineering
Department of Electrical Engineering

Shawana Tabassum, Ph.D., Committee Chair

College of Engineering

The University of Texas at Tyler
November

This is to certify that the Master's Thesis of

TANZILA NOUSHIN

has been approved for the thesis requirement on

9th November 2022

For the Masters of Science in Electrical Engineering

Approvals:

DocuSigned by:
Shawana Tabassum
AA11ECFB133F4AF...
11/9/2022

Thesis Committee Chair: Shawana Tabassum, Ph.D.,
Department of Electrical Engineering

DocuSigned by:
Premananda Indic
0EE7E374D15143B...
11/9/2022

Member: Premananda Indic, Ph.D.,
Department of Electrical Engineering

DocuSigned by:
Shih-Feng Chou
B32559E29B3244B...
11/9/2022

Member: Shih-Feng Chou, Ph.D.,
Department of Mechanical Engineering

DocuSigned by:
Hassan El-kishky
7E4401EB0BCF49D...
11/9/2022

Chair: Dr. Hassan El-Kishky, Ph.D.,
Department of Electrical Engineering

DocuSigned by:
3E50E32BE8F046A...
11/10/2022

Javier Kypuros, Ph.D.,
Dean, College of Engineering

Acknowledgments

All praise to almighty God for blessing me with success in my career. I would like to express my heartfelt gratitude and appreciation to my supervisor and committee chair, Dr. Shawana Tabassum for her intellectual guidance, continuous support, and motivation to face and overcome challenges. She was always there whenever I needed her no matter how much work she had. She taught me how to set goals in life and achieve them, she built the confidence in me that made me create my own identity. Without her support my research career and this thesis would have been impossible.

I am thankful my committee members, Dr. Premananda Indic and Dr. Shih-Feng Chou, for guiding me with their insightful knowledge and helping me in every step of my Master's journey. My deepest gratitude and credit for my career success goes to my mother and father for their continuous encouragement, prayers, and care for me. The person without whom I wouldn't have reached here today, is my husband, Md Sharif Ahmed. His everlasting love, support, and optimistic mindset gave me the strength to win over all the difficulties and hard times in my career and life.

Finally, I would like to thank my fellow labmates, Nafize, Alina, Suwarna, and Vivek for providing me with a friendly and productive research environment in the lab.

Table of Contents

List of Tables

List of Figures

Abstract

Inflammatory biomarkers present in the human body play a vital role in medical field by guiding the clinician in decision-making for many diseases. The levels of these inflammatory biomarkers are associated with the severity and progress of several diseases. Researchers have found that increasing severity of many diseases such as cardiovascular disease, after surgery infection, and adverse clinical outcomes due to infectious diseases, results in the elevation of the level of inflammatory biomarkers in human sweat. Furthermore, the inflammatory cytokines indicate the pathophysiology and prognosis of critically ill SARS-CoV-2 patients. In this thesis work, different sensors have been developed for the detection of inflammatory biomarkers, such as C-reactive proteins (CRP), Interlukin-6 (IL-6), and Interlukin-10 (IL-10) to enable real-time monitoring of the aforementioned disease conditions. These inflammatory biomarkers also provide valuable information on the wound healing progress. Hence, a wound monitoring sensor has also been fabricated in this thesis work for real-time monitoring and management of wound dynamics. Besides detection and monitoring the disease conditions, it is also necessary to provide controlled and on-demand drug delivery. Therefore, an electronically controlled drug delivery module was fabricated to deliver transdermal drug through the human skin. The developed sweat sensors detected the target analytes from a small amount of artificial sweat sample collected via a microfluidic channel that minimized the requirement of sweat sample, and reduced contamination and evaporation of sweat from the human skin. The microfluidic

channel collected the sweat from skin and directed the sweat flow to the main sensing region. In addition, a substantial amount of attention is needed to ensure the high-precision performance of wearable sensors irrespective of any body movements such as stretching, bending, and twisting motions. To achieve this, kirigami-patterned strain-insensitive sensors were integrated on a biaxially stretchable kirigami structure to quantitively measure sweat pH and temperature. The strain-insensitive sensor depicted an excellent performance under biaxial tensile strain applied up to 220% and torsional strain up to 360°. Finally, tattoo sensors, fully conformal like a tattoo on the skin, were fabricated. In order to validate the performance of the tattoo sensor on a living cell, the temperature and humidity data were collected from live plants under both water-stress and unstressed conditions. All the sensors reported in this thesis have impressive performance with high sensitivity, accuracy, and low limit of detection (LoD), which are the expected parameters for every sensor. The sweat sensors fabricated in this thesis depicted an excellent combination of flexible structure, cost-effective fabrication, skin conformity, and high linearity of response that make our devices introduce a promising new route in the healthcare application of skin-inspired wearable sweat sensors.

Publications

[1] **T. Noushin** and S. Tabassum, "Kirigami-Patterned IoT-Enabled Smart Anklet to Aid Physiotherapy of Patients with Foot Injury", accepted for Lecture presentation at the 2022 IEEE SENSORS conference, to be held in Dallas, Texas USA from Oct 30 - Nov 2, 2022.

[2] A. N. Pereira et al., "Flexible Sensor Suite Integrated Into Textile for Calcium Ion and Fall Detection," in IEEE Sensors Letters, vol. 6, no. 10, pp. 1-4, Oct. 2022, Art no. 2501004, doi: 10.1109/LSENS.2022.3210878.

[3] S. Karna, **T. Noushin,** and S. Tabassum, "IoT based Smart Helmet for Automated and Multi-parametric Monitoring of Underground Miners' Health Hazards," 2022 IEEE 15th Dallas Circuit and System Conference (DCAS), 2022, pp. 1-2, doi: 10.1109/DCAS53974.2022.9845621.

[4] **T. Noushin**, N. I. Hossain, **S.** Tabassum, "IoT-enabled Integrated Smart Wound Sensor for Multiplexed Monitoring of Inflammatory Biomarkers at the Wound Site" Frontiers in Nanotechnology, vol. 4, Jan 7, 2022. doi: 10.3389/fnano.2022.851041

[5] **T. Noushin,** N. I. Hossain, **S.** Tabassum, **"**Kirigami-Patterned Highly Stable and Strain Insensitive Skin pH and Temperature Sensors for Long-term Wearable Applications,". *HI-POCT, 2022*, March 10-11, **2022.** doi: 10.1109/HI-POCT54491.2022.9744070.

[6] **T. Noushin**, S. Tabassum, "WRRIST: a wearable, rapid, and real-time infection screening tool for dual-mode detection of inflammatory biomarkers in sweat," Proc. SPIE 11955, Microfluidics, BioMEMS, and Medical Microsystems XX, 119550,2 March **2022**; https://doi.org/10.1117/12.2606248

[7] **T. Noushin** and S. Tabassum, "Multiplexed Electrochemical Sensor for Real-Time Monitoring of Inflammatory Biomarkers," 2021 IEEE Sensors, **2021**, pp. 1-4, doi: 10.1109/SENSORS47087.2021.9639859.

[8] A. N. Pereira, **T. Noushin,** and S. Tabassum, "A Wearable, Multiplexed Sensor for Real-time and In-situ Monitoring of Wound Biomarkers," 2021 IEEE Sensors, **2021**, pp. 1-4, doi: 10.1109/SENSORS47087.2021.9639722.

[9] N. I. Hossain, **T. Noushin,** and S. Tabassum, "Leaf-FIT: A Wearable Leaf Sensor for In-Situ and Real-Time Monitoring of Plant Phytohormones," 2021 IEEE Sensors, **2021**, pp. 1-4, doi: 10.1109/SENSORS47087.2021.9639842.

Chapter One

Introduction

After seeing the entire world struggling with the COVID-19 pandemic, it is our opportunity and responsibility to use the lessons learned and experience we had to prepare ourselves for any upcoming pandemic by fabricating devices to rapidly detect, monitor, and ensure on-demand treatment for any infectious diseases, mitigate the spread of those infections and ensure a better management of such infectious diseases.

1.1 Inflammatory Biomarkers

A biomarker that provides information about inflammation is called an inflammatory biomarker. The immune system in our body responds to any perceived infection, injury, or toxin via a complex process. In response to an inflammation, our immune system releases specific cytokines, which are known as signaling molecules. The signals produced by cytokines activate more cells in our immune system, releasing even more of these cytokines. Some cells also release specific proteins activating other parts of our immune system. In severe inflammation, the immune system goes into a state of chronic condition or long-term inflammation. Patients with autoimmune diseases such as rheumatoid

arthritis, cardiovascular disease, lupus, after surgery infections, inflammatory bowel disease, diabetes, and heart disease struggle with inflammation conditions [1].

1.2 Association of Inflammatory Biomarkers with Diseases and Wound

Clinicians get an idea about disease prognosis by detecting inflammatory biomarker levels and find out possible causes of symptoms. If the levels of inflammatory biomarkers are out of bound, it indicates that the patient might have a disorder caused by inflammation. For example, in cancer patients, if the inflammatory biomarkers levels are high, then the patient will have an increased risk of death. In order to get a more accurate understanding of inflammation conditions, it is essential to monitor more than one inflammatory biomarker. Different inflammatory biomarkers provide specific and slightly different information on the health status.

1.2.1 C-reactive Protein (CRP)

CRP protein is known as acute phase reactant that is released in response to an inflammation. The level of CRP is elevated in several inflammatory conditions, many bacterial or viral infections such as pneumonia, different autoimmune diseases like lupus or rheumatoid arthritis, chronic inflammation, cancer, and cardiovascular diseases [2]. In addition, CRP provides valuable information on wound healing progress [3].

1.2.2 Interlukin-6 (IL-6)

IL-6 interleukin is mainly produced by T-lymphocytes and macrophages in response to pathogens and is a pivotal biomarker in detecting several viral infections. Furthermore, IL-6 biomarker is released in response to hyper-inflammation caused by severe acute respiratory syndrome coronavirus 2 (SARS-CoV-2). Elevated levels of IL-6 indicate disease severity and possibility of death. IL-6 is considered as a particularly important biomarker in the COVID-19 pathogenesis because it is positively correlated with disease severity, treatment stages and radiologic changes. By quantifying the level of this biomarker, the clinicians can predict the need for mechanical ventilation [4]. In addition, IL-6 is involved with skin wound healing as the IL-6 levels in wound fluids is correlated with wound-healing progress rates [5].

1.2.3 Interlukin-10 (IL-10)

The importance of IL-10 as an inflammatory biomarker in diagnosis and treatment of severe COVID-19 disease has emerged. Together with IL-6, high levels of IL-10 can more accurately predict possible outcomes in severe/critically ill COVID-19 patients. Researchers have found significantly higher IL-10 concentrations in COVID-19 patients admitted to intensive care units (ICU) in comparison to the non-ICU patients. Furthermore, IL-10 concentrations are strongly correlated with other inflammatory

markers such as IL-6 and CRP and the levels of all these biomarkers can predict the status of the diseases with a higher accuracy [6, 7].

Researchers have found that increased levels of IL-10 are associated with higher rate of tumor growth and recognized IL-10 as an important biomarker for cancer disease [8]. Furthermore, elevated IL-10 levels can impede wound repair, whereas IL-10 deficiency in the blood results in an accelerated wound closure [9].

1.3 Sweat Biofluid Collection Via Microfluidic Channel

Significant research efforts have been made in the development of wearable technology for detecting and real-time monitoring of biomarker levels in accessible biofluids such as saliva, tears, urine, and sweat. Sweat is considered to be an ideal candidate for prolonged, nonobtrusive, noninvasive and semicontinuous health monitoring because of being a continuously accessible biofluid and containing physiological and metabolic information [10].

1.3.1 Sweat Biofluid

In recent years, wearable sweat-sensing platforms have attracted the attention of researchers worldwide. A fully integrated wearable sweat patch consists of two components: the sweat collector and the sensor. The choice of designing the sweat-collection mechanism is dependent on the amount of sweat produced by the user. For

instance, a wearable sweat sensor designed for athletes should have the capacity to collect a sufficiently large volume of sweat and capable of removing the sweat to facilitate the next round of collection. In contrast, a wearable sweat sensor designed for inactive patients admitted to the hospital should have a sweat-collection mechanism that works with a minuscule amount of sweat [10].

1.3.2 Microfluidic Channel

A very crucial part of the wearable sweat sensing is the collection of the test sample, which is eccrine sweat in this work. The goal is to transport the sweat that originates from the eccrine sweat glands towards the sensing regions where the concentration of the target analytes is measured.

Microfluidic channel is most commonly used in wearable sweat sensors to collect and transport small volume of sweat sample. Microfluidic channel enables precise control of sweat flow and confinement of the sweat sample in micro/nanoliters volume. Inside this channel, a capillary force governs the transport of the biofluid. Generally, the microfluidic architecture consists of channels and chambers, such as inlets and outlets. The function of inlets is to collect the sweat from skin surface and direct it towards the sensing part for successful detection of biomarkers. The outlets are designed to direct the sweat out of the sensing part so that a new sweat keeps flowing at a specific time interval. In this way, the

changes in the concentration of biomarkers in sweat can be detected and monitored continuously in real-time.

The design of the microfluidic channel should be straightforward and the best suited fabrication techniques should be adopted depending on the design of the sensor. The microfluidic channel integrated with wearable sensor consists of multiple layers, such as multiplexed sensors scribed on a flexible substrate, a microfluidic channel with outlets and inlets patterned on a double-sided adhesive layer [10, 11].

1.4 Sweat pH and Skin Temperature Monitoring

Eccrine sweat pH and skin temperature can be measured noninvasively with wearable sweat sensors to diagnose and aid in continuous monitoring of a wide range of physiological conditions. Measurement of sweat pH and skin temperature for continuous and real-time health monitoring provides valuable information about fitness and wellness [12].

1.4.1 Sweat pH

Besides the inflammatory biomarkers, variations in sweat pH (i.e., acidity or alkalinity) indicate whether the body is dehydrated and indicate skin conditions such as dermatitis, acne, and other skin infections. In diabetic patients, monitoring of sweat pH can save patients from life-threatening conditions. Moreover, if the diabetic patient is going

through a low level of blood glucose for a prolonged period of time followed by excessive sweating at night, that can be detected by a high level of sweat pH. As a result, an immediate medical intervention can take place [13].

1.4.2 Skin Temperature

For real-time monitoring of the patient's hydration, measuring skin temperature together with sweat pH continuously, can provide more accurate data on patient's health [14]. Furthermore, an elevated body temperature indicates a wide range of disease conditions such as COVID-19 [14]. The final goal of measuring skin temperature is to complement the biomarker monitoring and determine the disease severity and find out when there is a need to intervene.

1.5 Strain-insensitive Structure

Wearable sensors are exposed to body movements, such as stretching, twisting, flexion, and extension. Therefore, it is crucial to achieve reliable detection of inflammatory biomarkers and pH levels in sweat irrespective of body movements. Kirigami-like structures inspired by Japanese traditional paper-cutting art, has created a new dimension in the field of flexible and wearable devices by featuring a stretchable and deformable framework. In order to achieve stable electrical signals from a skin-conformal device, it is compulsory to decouple desired output signals from mechanical stretchability-induced

electrical signal due to the changes in body movements. Kirigami structures create a reconfigurable morphological response that enables superior stretchability and strain-insensitive response under stretching or mechanical deformations. Furthermore, kirigami-inspired wearable sensor design features notches to tune the stiffness of flexible devices in order to improve surface conformity and breathability onto human skin. Under mixed applied strain, such as high tensile and torsional strain states, strain-insensitive response of the sensor is achieved by uniformly redistributing stress concentrations away from the active sensing elements via cuts and notches [15-17].

1.6 Drug Delivery

In the drug delivery process, the required drug is introduced into the patient's body for a desired period of time at a specific rate. It is important that the drug concentration in the blood is maintained at a specific level to ensure the maximum therapeutic benefit. There are different categories of controlled drug delivery systems: oral systems, intravenous, and transdermal drug delivery. The disadvantages of oral route include poor absorption, bioavailability, and drug degradation [18].

On-demand drug delivery by releasing drug molecules from wearable biomedical devices enables targeted dosing with precise control to meet treatment requirements for different therapeutic applications.

Electrically stimulated transdermal drug delivery systems are an attractive alternative because of non-invasiveness, ease of delivery, personalized, safe, and better pain management. With this approach, continuous drug monitoring and delivery has the prospective to become a promising alternative to current therapeutic strategies.

1.7 Overview of Thesis

This thesis project reports different skin-interfaced wearable devices integrated with a microfluidic channel and a strain-insensitive kirigami structure for the detection of inflammatory biomarker levels, skin temperature and pH levels in human sweat. The device will be used to monitor the health conditions of patients with cardiovascular, infectious, or viral diseases. The device also includes a drug delivery component for electrically controlled drug delivery in real-time to provide immediate treatment and save lives in emergency situations. Finally, this work presents a tattoo sensor that can be attached on a skin like a tattoo. The reported sensors have a strong potential to monitor inflammatory biomarkers in sweat and improve the treatment management in real-time. The tattoo sensor was functionalized for temperature and relative humidity detection and monitoring on the leaves of a live plant. The sensor monitored vapor-pressure deficit (VPD) providing valuable information on plant transpiration. Different types of wearable sensors developed in this thesis are summarized below:

- Development of a silicon-based multiplexed sensor functionalized with selective coatings for inflammatory biomarkers detection and monitoring

- Fabrication of a screen-printed flexible and wearable sweat sensor integrated with microfluidic channel for the detection and monitoring of inflammatory biomarkers

- Development of a strain-insensitive kirigami-inspired flexible sensor with improved skin conformity for measuring sweat parameters irrespective of body movements such as stretching, bending, twisting, or shearing.

- Development of a wound sensor for wound status monitoring by continuous detection of wound biomarkers in wound fluid

- Fabrication of a fully skin-conformal tattoo sensor for prospective detection of inflammatory biomarkers in sweat and continuous monitoring of disease progression. The performance of the tattoo sensor was validated in live plants by monitoring the temperature, relative humidity (RH), and vapor-pressure deficit (VPD) in real-time.

Chapter Two

Development of Functionalization Coatings

This chapter aims to give an overview of preparation and verification of functionalization coatings for the detection of target biomarkers.

2.1 Literature Survey

There have been numerous ongoing researches on developing improved diagnostics and therapeutics for COVID-19 and other emerging infectious diseases. Following the recent research trend, this thesis is focused on detecting the infectious diseases at an early stage (e.g., 1-7 days ahead). Our developed sensor has the potential to detect biomarkers in less than one minute at the point-of-care. By ensuring early detection, patients can be isolated, and the treatment can be started immediately that will in turn mitigate the spread of an infection. It is important to monitor the recovery process of viral infection in both symptomatic and asymptomatic patients. Even if the patients are found to have a low concentration of antibodies, it might hinder the recovery process because of the deficiency in cellular immunity [19]. In contrast to the current diagnostic methods, point-of-care tests have the potential to cope up with the exponential spread of COVID-19 virus by enabling earlier detection of disease, easier

monitoring at the bedside or in a remote area without the requirement of trained personnel [20]. Various laboratory-based techniques have been developed to detect the COVID-19 infection including enzyme-linked immunosorbent assay (ELISA) [21], reverse transcription real-time quantitative polymerase chain reaction (RT-qPCR) [22-24], clustered regularly interspaced short palindromic repeats (CRISPR) [4], chemiluminescence immunoassay (CLIA) [20], and lateral flow immunoassay (LFIA) [25].

The ELISA method requires the collection of a large volume of blood sample, which is invasive, particularly for infants and kids [26 ,27]. RT-qPCR and CRISPR need to go through multiple sample processing steps in a laboratory setup that makes it a slow technique (up to two weeks or longer). Therefore, these methods have limitations in handling cities with fast-growing number of COVID-19 patients. Moreover, the accuracy of the test is compromised with the high mutation rate of virus in the target genomic region [19]. The LFIA-based test kit detects viral COVID-19 antigen from nasopharyngeal swab within 10–30 min [20], however, this method lacks continuous real-time monitoring of the infection level that will guide doctors in adjusting the treatment procedure and following up on the healing progress of the patients. Moreover, detection of the level of only one inflammatory biomarker in viral or bacterial infection may lead to false positives/negatives.

To address these challenges, our multiplexed sensor comprised of four working electrodes is capable of quantifying the levels of four inflammatory biomarkers that get elevated in patients infected with COVID-19 or other infections. The four biomarkers include Interleukin-6 (IL-6), Interleukin-10 (IL-10). procalcitonin (PCT), and CRP [27, 28]. In this work the sensor was functionalized to detect and

monitor two inflammatory biomarkers including CRP and IL-6 at the same time on a single chip. This sensor will allow diagnosis and prognosis of the disease accurately, rapidly, and non-invasively. Additionally, this sensor will ensure efficient control and management of emerging infectious diseases by providing an early detection of any viral and/or bacterial infection so that patients can get the appropriate treatment right away and quarantine themselves to protect others.

2.2 Sensor Structure and Working Principle

Our screen-printed electrochemical sensor consists of 4 working electrodes (WE) for detecting 4 biomarkers, one reference electrode (RE), and one counter electrode (CE) (Fig. 1). The WE and CE are made of gold and RE is made of Ag/AgCl. The WE will measure the levels of biomarkers (CRP and IL-6). Being made of gold, the CE will be chemically inert providing the electrons a path to flow. The RE mainly provides a stable point for reference redox potential. Gold nanoparticles decorated multi-walled carbon nanotube nanocomposite (Au-MWCNT) was formed on each WE to create a three-dimensional working electrode surface to enhance the sensitivity. The Au-MWCNT functionalized WEs were immobilized with specific antibodies to detect the specific biomarkers.

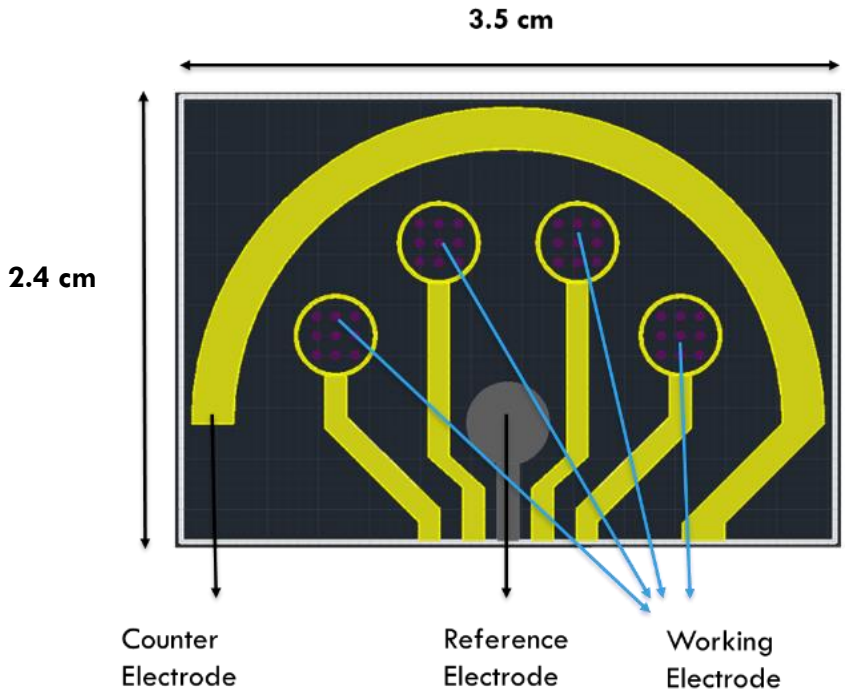

Fig. 1: Silicon-based sensor with four Working Electrodes, one Counter Electrode and one Reference Electrode

2.3 Sensor Development with Functionalized Coatings

Different coatings were made in the fabrication process of this sensor (Fig. 2). The preparation details and significance of each coating are given in the following:

The electrolyte solution was composed of both the oxidized and reduced forms of iron, namely, potassium ferrocyanide and potassium ferricyanide, which were mixed in 1:1 ratio using PBS pH 7.4 buffer. This electrolyte ensured current flow through the working and counter electrodes. Gold Decorated MWCNT Modified Electrode were prepared by following the reduction process of

$HAuCl_4.H_2O$ with sodium citrate described below. 8 μL of this solution was taken, drop-casted on the WE and left to dry for 3 hrs [29].

To prepare the Au-MWCNT solution, firstly 0.01% $HAuCl_4$ was brought to boiling point, to which 1.0% sodium citrate was slowly added under stirring and left to react for 15 min. Then the solution was centrifuged at 14 000 rpm for 20 min to purify the gold nanoparticle dispersion and remove the remaining traces of unreacted $HAuCl_4$ and sodium citrate followed by redispersion of the precipitated solid in Milli-Q water. Modified MWCNTs were synthesized by treating the MWCNT in 3M HNO_3 Acid Solution under continuous stirring for 24 h. Afterwards, the MWCNTs were thoroughly washed with Milli-Q water and dried for 12 h.

For the functionalization of the gold nanoparticles, 1% (v/v) Acetic Acid solution was prepared,

and 1% (w/v) chitosan was dissolved in that Acetic Acid Solution. 0.5% (w/v) dried Au-MWCNT nano particles were mixed into that Acetic Acid and Chitosan solution and sonicated for 8 hrs [29].

1mM of linker acid ($HS(CH_2)_4–COOH$) solution was prepared in pH 7 PBS Buffer, 8 μL of which was drop coated on the Au-MWCNT layer. This Linker Acid coating binds the EDC-NHS in the antibody to the MWCNT-AuNP layer perfectly [29].

For antibody immobilization, a 1:1 solution of EDC and NHS was prepared, followed by adding the mixture to 1mg/mL of anti-CRP solution. 8 μL of the anti-CRP solution was coated on the WE and kept at 7° C for 12 hours so that the antibody attaches and immobilizes to the surface [29].

A bovine serum albumin (BSA; 2 mg mL^{-1}) solution was drop coated on the sensor to block the non-specific sites so that the protein doesn't get attached to non-specific molecules and get attached to antibody only. The list of all functionalization coatings is given in Table 1.

CRP Protein was reconstituted at 100 µg/mL concentration and fourteen different concentrations were prepared for target protein detection. After each functionalization step, the electrochemical measurement was taken. For example, electrochemical readings were recorded for bare sensor, Au-MWCNT Coating, Acid Coating, Antibody, and BSA coating. Finally, measurements were recorded when the sensor was exposed to CRP concentrations ranging from 1 femtomolar (1 fM) to 1 micromolar (1 µM). The cut-off concentration of CRP in healthy person is <10mg/L (~ 0.8 µM) whereas in infected body this CRP level gets elevated.

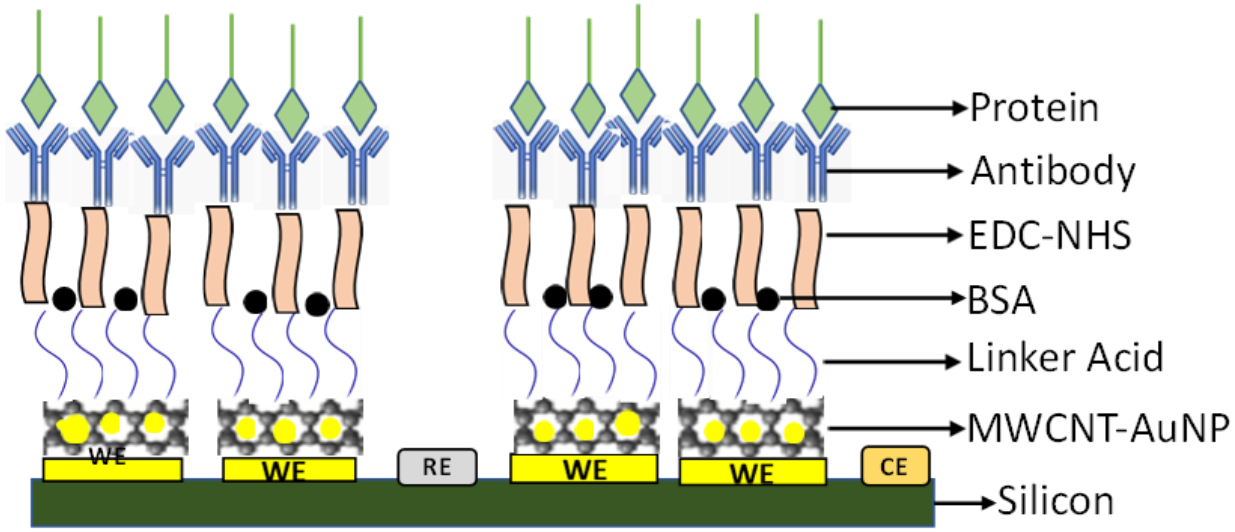

Fig. 2: Cross-sectional view of the sensor with surface functionalization coatings: MWCNT-AuNP, Linker Acid, Anti-body, and BSA

Table 1: List of Functionalization Coatings with Purpose

Coatings	**Purpose**
Coating 1: Gold Decorated MWCNT	Increases the surface area
Coating 2: Linker Acid	Binds to the antibody
Coating 3: Antibody	Provides selective detection
Coating 4: BSA	Blocks non-specific molecules

2.4 Experimental setup

The three electrodes of the sensor were connected to a benchtop potentiostat using alligator clips and results of electrochemical tests (Cyclic Voltammetry, Chronoamperometry) were displayed on the screen of a smartphone via Bluetooth (Fig. 3). In this small-spaced experimental setup, the infection level detection can be done at the bedside or in a remote area within one minute without any requirement of trained personnel.

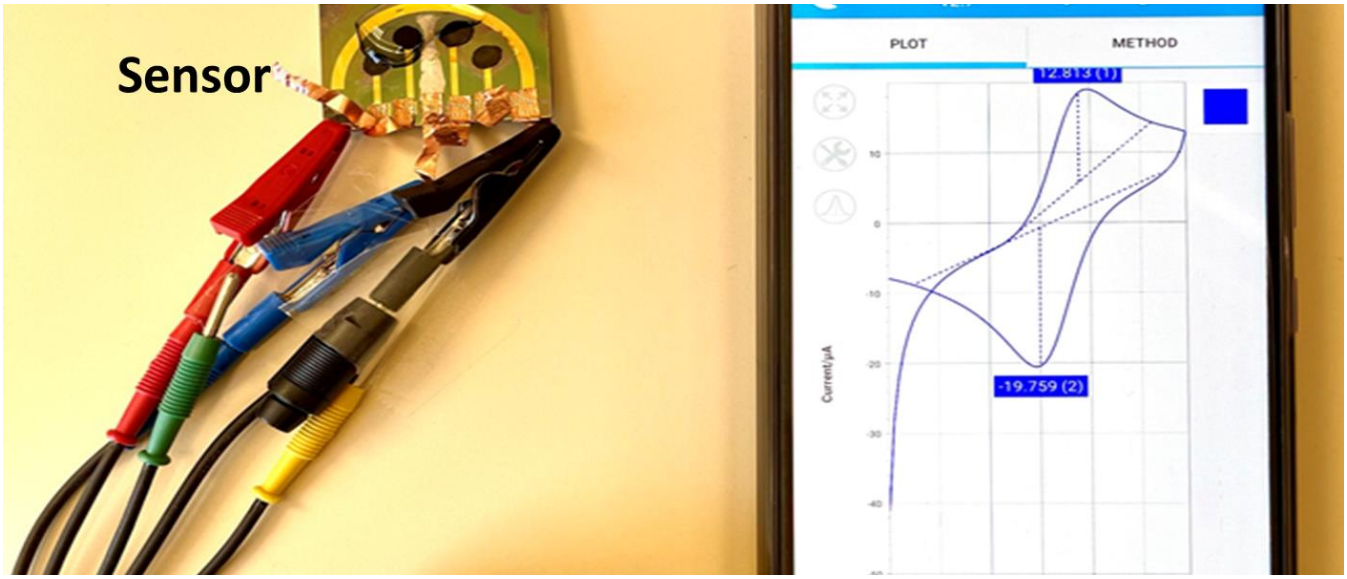

Fig. 3: Experimental setup of the sensor, wherein the data was collected by a benchtop potentiostat and displayed on a smartphone.

2.5 Electrochemical Characterization

We conducted all the electrochemical measurements using a benchtop potentiostat. For the electrochemical characterization of redox activity, we conducted cyclic voltammetry (CV) scans for different functionalization coatings on the WE surface, as shown in Fig. 4a. The MWCNT-AuNP-coated electrode exhibited a 10-fold enhancement in redox current, eventually increasing sensitivity of the sensor. The redox current of the electrode decreased with the immobilization of additional coatings because of the insulating property of the layers. As a result, electron transfer through the electrodes slowed down.

Next, we employed chronoamperometry (CA) to characterize the response time for both the MWCNT-AuNP-coated and bare sensors by applying a constant potential of 0.4 V to WE with

respect to RE (Fig. 4b), where it's evident that the response time for the sensor without MWCNT-AuNP coating is ~0.04s and for the sensor with MWCNT-AuNP coating is ~0.08s. The MWCNT-AuNP coated sensor depicted a delay in response time due to the diffusion of charge carriers through the three-dimensional CNT matrix. However, 0.08s is a significantly faster response time compared to many other nanostructured sensors reported in the literature.

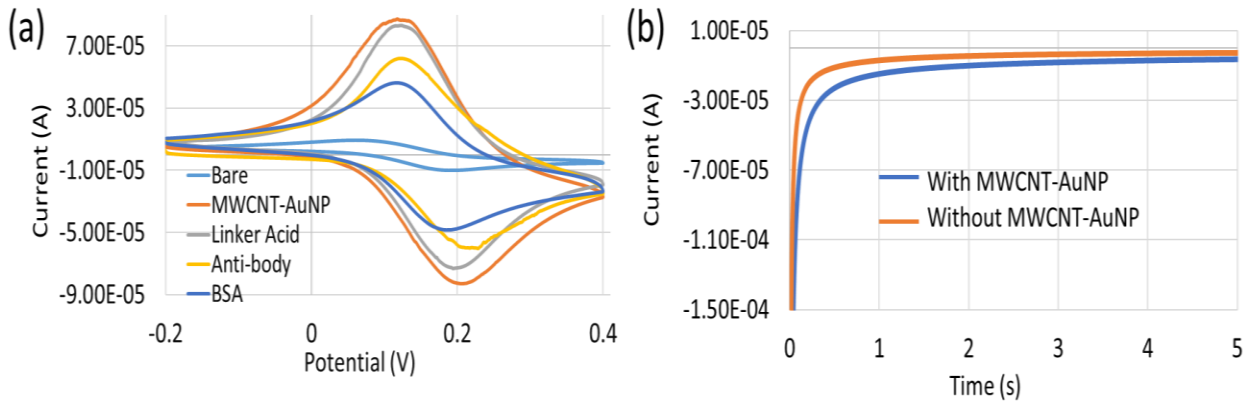

Fig. 4: (a) CV curves in response to different functionalization layers on the working electrode; (b) CA responses with and without the MWCNT-AuNP coating on the working electrode

2.6 Electrochemical Measurements of CRP Biomarker

We have demonstrated the detection of CRP protein with our sensor using a small volume of sample (~100 μL). The CV responses for fourteen different concentrations of CRP, ranging from 1 femtomolar to 1 micromolar is depicted in Fig. 5a where it's evident that with the higher concentration of CRP protein, the current flow between WE and CE is decreasing. This reduction in the redox current took place because of the formation of a

thicker insulating layer of immunocomplex with increasing concentration via binding a larger number of CRP protein molecules with the anti-CRP coated sensor surface.

The calibration plots for both the sensor with MWCNT-AuNP coating and without MWCNT-AuNP coating are shown in Fig. 5b. The current is inversely proportional to the CRP concentration. The slopes of the calibration curves are 1.375 and 0.912 $\mu A\ \mu M^{-1}$, the sensitivity 10.95 and 7.26 $\mu A\ \mu M^{-1}\ cm^{-2}$, and limit-of-detection (LoD) 0.0066 and 0.9 femtomolar (cut-off CRP level in healthy person is ~0.8 μM, whereas in infected person it gets elevated) for the sensors with MWCNT-AuNP coating and without MWCNT-AuNP coating, respectively. To calculate the LoD, we employed the following equation [29].

LoB = Mean of signal (blank sample) + 1.645 × (Std dev of blank sample)

Limit-of-detection of the signal (YLoD) = LoB + 1.645 × (Std dev of target at low concentration)

LoD = (YLoD - c)/slope of the calibration curve

The MWCNT-AuNP coated sensor also demonstrated an impressive selectivity (Fig. 5c) against interfering species typically present in blood plasma, namely IL-6 (0.1 nM), Glucose (5 mM), and cortisol (0.4 μM). When the sensor was exposed to the mixture of interferent molecules without any presence of CRP, there was no significant change in the current response w.r.t. the current for blank sample (i.e., absence of any biomolecules), proving to be promising device for the detection and continuous and real-time monitoring of infection level.

The sensor was further examined for repeatability (Fig. 5d) showing a consistent current level for 1 pM CRP at three consecutive days. Moreover, the reproducibility test (Fig. 5e) shows that for four consecutive weeks, the performance of the sensor was consistent showing the same current level for 1 pM CRP, proving that our sensor is reusable over a month. There was an excellent linear agreement (Fig. 5f) between the sensor-measured CRP level and reference CRP level.

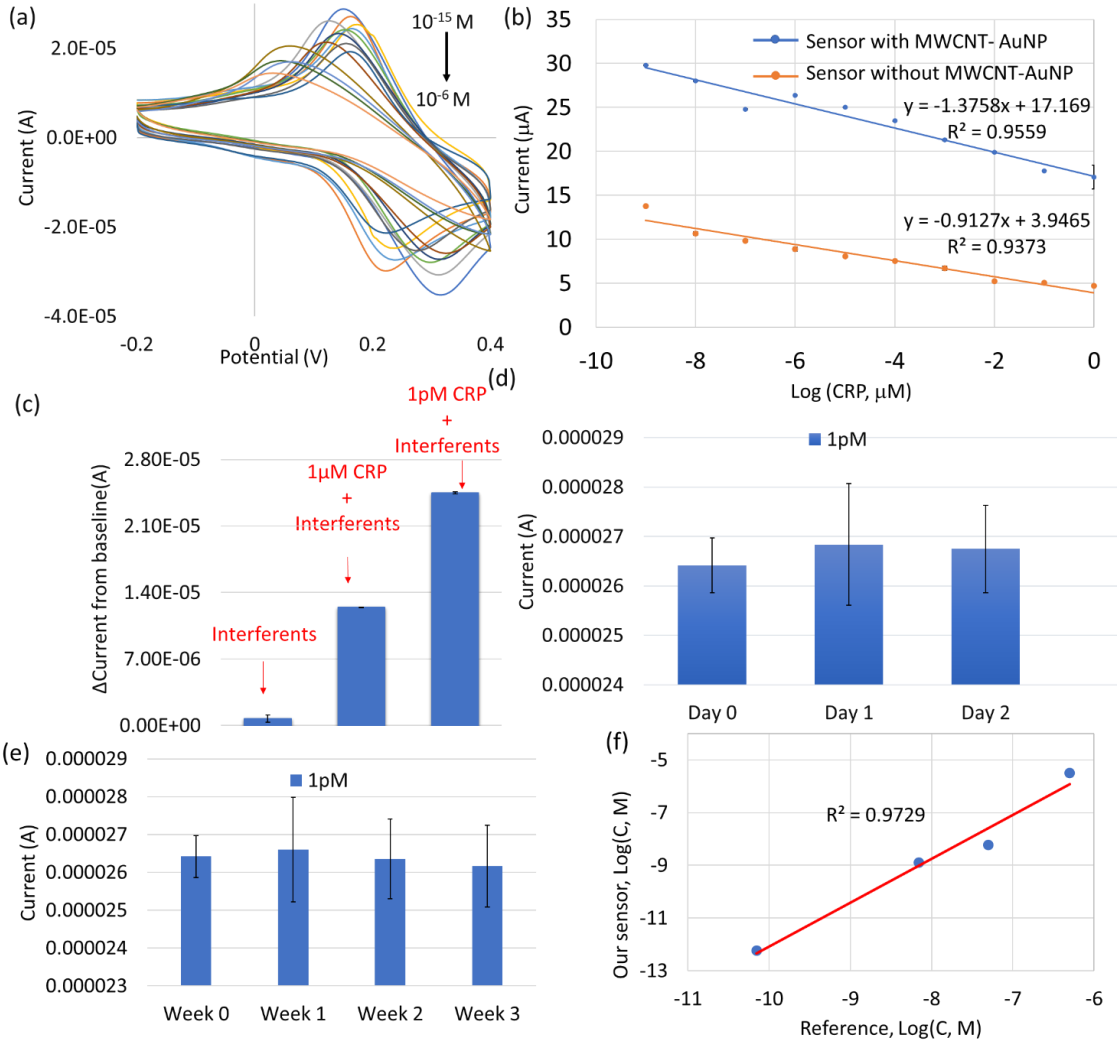

Fig. 5: (a) CV responses of the sensor for CRP concentrations ranging from 1 fM to 1μM in PBS (pH=7.4); (b) Calibration plot of the sensors with MWCNT-AuNP coating and without MWCNT-AuNP coating. Error bars represent 3 repeated measurements with the sensor; (c) Selectivity test: current variations w.r.t. the baseline current for the blank sample, in presence of specific CRP concentrations (1 μM and 1 pM) and the nonspecific interferents, Interleukin-6 (0.1 nM), glucose (5 mM), and cortisol (0.4 μM); (d) Repeatability test: in response to the CRP concentrations (1 pM) for three consecutive days; (e) Reproducibility test: in response to the CRP concentrations (1 pM) for four consecutive weeks. (f) Agreement between the developed sensor and reference.

2.7 Summary

In this work, a user-friendly, high-performance, and rapid point-of-care sensor was developed for non-invasive infection level detection and continuous monitoring of the recovery process. This research project developed the biofunctionalization coatings on a novel biochip for rapid and real-time detection of infection at the point-of-care. The biochip features multiplexed detection of 4 inflammatory biomarkers using electrochemistry-based measurement techniques. We have demonstrated the detection of C-reactive proteins (CRP), an inflammatory biomarker, elevated levels of which is found to be associated with cardiovascular disease, mortality after vascular surgery, adverse clinical situations, and death in critically ill COVID-19 patients. We have functionalized the working electrodes (WE) with Gold nanoparticles (AuNPs) decorated multi-wall carbon nanotube (MWCNT) so that the protein biomarkers are selectively captured on the respective WEs depending on

the protein-antibody binding ensuring higher sensitivity. The sensor demonstrates a sensitivity of 10.95 $\mu A\ \mu M^{-1}\ cm^{-2}$, a limit of detection of 0.0066 femtomolar, and a response time of only 0.08 seconds. Our research holds potential to benefit the society by reducing the time to detection, especially in an under-resourced setting and save lives. Moreover, our device has huge potential to manage future pandemics through early diagnosis and timely treatment and isolation.

Chapter Three

Screen-printed Flexible Sweat Sensor Integrated with Microfluidic Channel for Inflammatory Biomarkers Detection

3.1 Literature Survey

Chronic conditions, including diabetes, cognitive impairment, arthritis, heart disease, and other inflammatory conditions get severe in adults as they age and in younger population as they become more obese. Elevated levels of inflammatory cytokines such as interleukin-6 (IL-6) is identified as one of the most efficient cytokine predictors of all-cause mortality. Therefore, continuous monitoring and detection of IL-6 levels with high sensitivity plays a vital role in improving the health condition of patients suffering from chronic diseases. A wearable and flexible sensor integrated with wireless data transmission to a smart device has huge potential to ensure real-time healthcare monitoring with good compatibility and lower installation costs. For these sensing devices, a non-obtrusively accessible biofluid must be chosen that can be an ideal candidate for prolonged and semicontinuous health monitoring [30].

Sweat is a clear, odorless substance, rich in physiological information and contains 99% of water and other molecules including Interleukin-6, cortisol, neuropeptide Y, and electrolytes. Unlike saliva, urine, or blood, the collection process of sweat is not cumbersome. Additionally, sweat

collection and monitoring is noninvasive and doesn't require specific laboratory facilities or well-trained personnel. Moreover, saliva specimens are influenced by dental and gingival diseases and require multiple collection throughout the day. Urine samples increase study burden requiring 24 h of processing in special laboratory and cold storage facilities. However, sweat sensor offers a reliable, non-occlusive, and noninvasive detection, overcomes circadian timing issues and offers a great potential to effectively monitor inflammation and chronic diseases [30].

Firstly, a wearable sweat sensor requires a convenient sweat collection method. Among the three major categories, namely, microfluidic collection, absorption collection, and direct on-skin collection, microfluidic channel provides precise control, flow, and confinement of micro/nanoliters of fluid at a comparatively smaller space. Among electroanalytical and optical sensing technologies, electroanalytical technology is preferred because optical technology shows deviations with nonuniformity of color and requires bulky and dark measurement setup. In contrast, electroanalytical technology is more stabilized and more suited for continuous measurements [30].

3.2 Device Fabrication and Biofunctionalizations

This paper reports a flexible sweat sensor integrated with microfluidic channel facilitating low-cost fabrication, wearer's comfort, and high sensitivity in multiplexed detection and monitoring of inflammatory biomarkers. Our sensor is fabricated on a polymer sheet comprised of two working electrodes (WEs), one reference electrode (RE) and one counter

electrode (CE). The WEs and CE were made of graphene ink and the RE was made of Ag/AgCl paste using a screen-printing technique [30].

Our device contains three layers, including large multi-inlet two-sided adhesive medical tape, one-sided thin medical tape, and multiplexed sensor scribed on the polymer substrate as depicted in Fig. 6a. The layer with large inlets was attached to the skin at one side and to the microfluidic channel on the other side. The adhesive side of the second layer was attached to the sensor that was visible on top of the skin in Fig. 6b. The flexible feature of the device matched with the non-planarity of human skin. The flexibility of the sensor is shown in Fig. 6d. As sweat started flowing into the device through the microfluidic channel shown in Fig. 6e-g, the electrochemical analytical techniques such as Cyclic Voltammetry and Chronoamperometry were performed for real-time monitoring at the bedside without requiring any trained personnel.

At first, the electrochemical co-deposition was performed in an aqueous solution of Prussian blue (PB) and gold nanoparticles integrated multi-walled carbon nanotube (AuNP-MWCNT) containing $K_3[Fe(CN)_6]$, $FeCl_3$, KCl, HCl and 1 mg mL^{-1} AuNP-MWCNTs by running two hundred voltammetry cycles over −0.3 to +1.2 V potential range and 0.05 V/s scan rate at room temperature [30].

The biofunctionalization of WEs prior to sensing different concentrations of biomarkers was carried out in several steps. Firstly, 1 mM of thiol cross-linker (HS $(CH_2)_4$–COOH) acid solution was drop coated to facilitate binding of antibody over AuNP-MWCNT layer. Next, an antibody solution was

prepared using EDC/NHS activation process and drop coated over the acid coating to ensure selective detection of target biomarker. After that, bovine serum albumin (BSA) solution was drop coated on the WEs to block non-specific binding sites. Artificial sweat (AS) was prepared using 85 mM NaCl, 13 mM KCl, 17 mM lactate and 16 mM urea in pH 7.4 buffer [30].

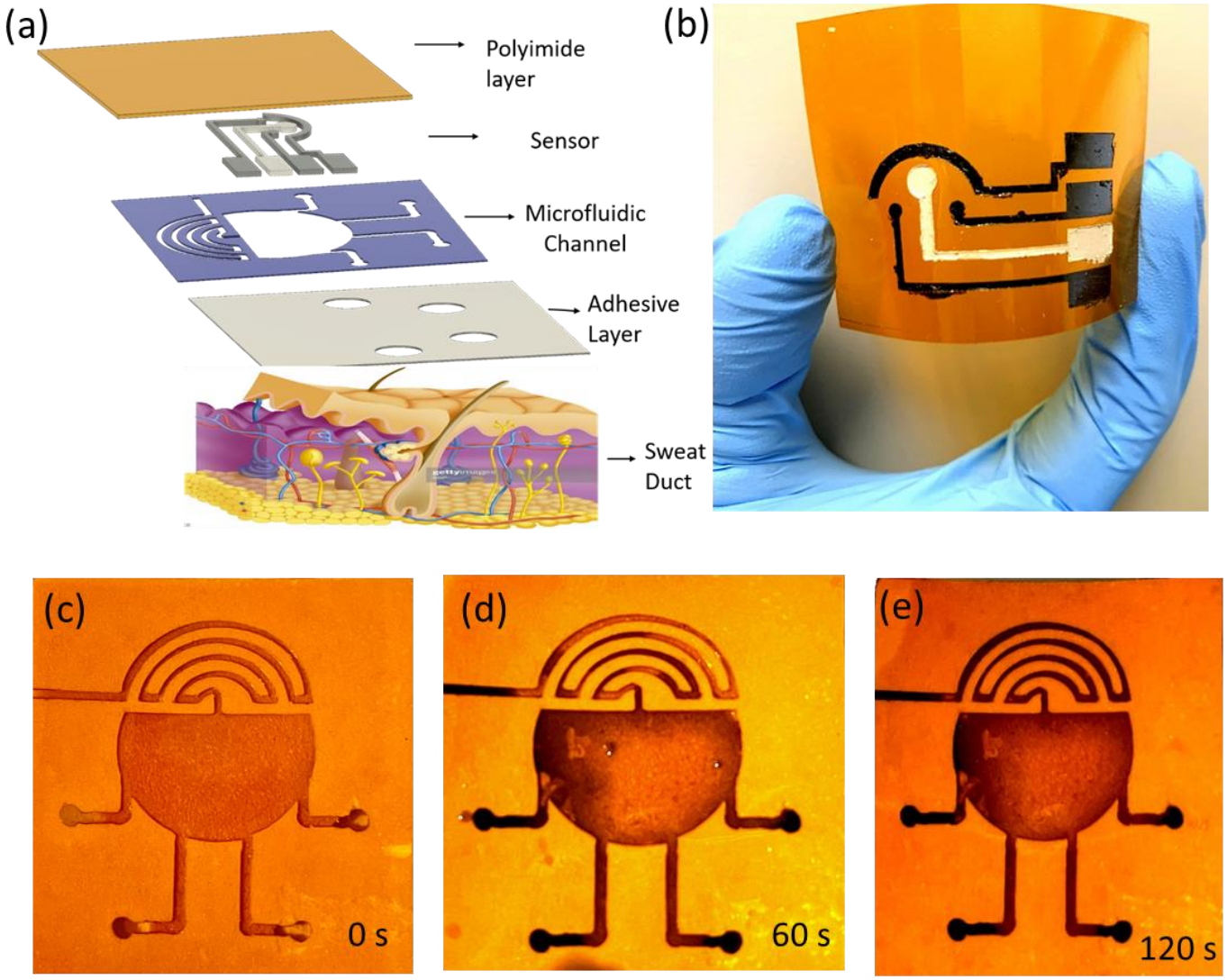

Figure 6. (a) Layers of sensor with the microfluidic channel in contact with skin (bottom) and sensor located at the top layer; (b) Photographic image of flexible skin patch; (c) Photographic

image of the beginning of sweat secretion process; (d) Microfluidic channel partially filled with artificial sweat; (e) Continuous sweat flow through the microfluidic channel

3.3 Results and Characterization

While several functionalization coatings were added to the WEs, the redox activity was characterized by applying CV technique as shown in Fig. 7a. The AuNP-MWCNT coating enhanced the redox current significantly as compared to the planar electrode and the oxidation current peak decreased due to the insulating layer formed on the WEs surface with each coating added.

Finally, the sensor integrated with the microfluidic channel layer was tested for eight varying concentrations of IL-6 protein starting from 0.1 pg/mL up to 1000 pg/mL that falls within the normal IL-6 level in the sweat (5–15 pg/mL) of a healthy person. Fig. 7b shows that with the increasing concentration of IL-6 protein, oxidation peak current was decreasing due to the dielectric property of protein molecules. The calibration curve shown in Fig. 7c was found by plotting CV oxidation peak currents vs. IL-6 concentrations.

To evaluate the selectivity of our sweat sensor, we tested the sensor with two different AS solutions, one with 10 pg/mL IL-6 and another without any IL-6 protein, but both containing a mixture of interferents such as 180 g/L glucose, 100 ng/mL cortisol, and 10 pg/mL CRP, typically found in a healthy individual's sweat [30]. In the absence of the IL-6, the current level was similar to the current level with zero target protein, whereas with the presence of 10 pg/mL of

IL-6, the sensor selectively detected the target protein and depicted a significant difference in the current level with respect to the blank sample as shown in Fig. 7d.

The CA plot with and without AuNP-MWCNT is depicted in Fig. 7e indicating that the sensor with AuNP-MWCNT coating has higher redox current and response time of 2s compared to the one without AuNP-MWCNT coating with a response time of 1.5 s. This higher response time was due to diffusion of charge carriers.

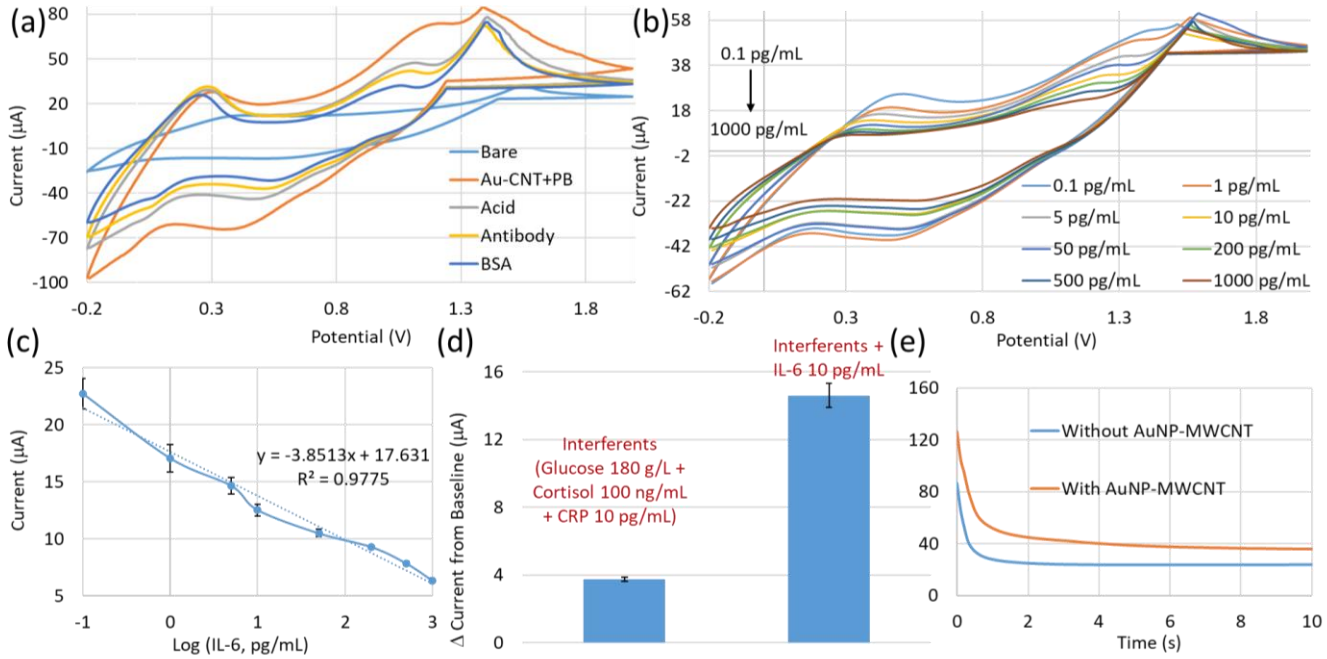

Fig. 7: (a) CV response with different functionalization coatings; (b) CV response for different IL-6 concentrations from 0.1 pg/mL to 1000 pg/mL; (c) Calibration curve with error bars representing three repeated readings; (d) Selectivity test in presence of interferents; (e) CA response with and without the AuNP-MWCNT coating.

3.4 Summary

In this paper, we have presented a novel method of the collection and detection of cytokines using a wearable and flexible sensor integrated with microfluidic channel. The integrated device depicts a high detection capability and continuous monitoring features. The fabrication process, materials, and substrates used for this sensor and microfluidic channel layers are cost-effective and simple proving our sensor to have high potential to be manufactured in large-scale and provide effective healthcare applications in under-resourced settings and rural areas. Therefore, our skin patch will aid in rapid detection and monitoring of biomarkers at the bedside ensuring multiplexed sensing with a high sensitivity of 122.59 μA $(pg/ml)^{-1}$ cm^{-2} and a limit of detection (LoD) of 0.886×10^{-3} pg/ml. The sensor is wearable on arm just like a small adhesive bandage.

Chapter Four

Strain-insensitive Kirigami Designed Skin Patch for Detection and Monitoring of Sweat pH and Skin Temperature

4.1 Literature Survey

Over the past decade, electronic skin (e-skin) has attracted a lot of interests in realizing soft, flexible, skin-like devices for continuous monitoring and therapeutic applications. Efforts are underway to enhance the sensitivity, flexibility, stretchability, and conformability of the e-skin devices. Some recent successes in this field range from tapping into the existing fabrication techniques to developing new materials such as conductive electrode material patterned on a spaghetti-like mesh of polyvinyl alcohol; flexible organic polymers and electronic components designed from the molecular level; wireless, biodegradable sensor that can be wrapped around blood vessels for blood flow monitoring; and metal oxides blended with stretchy rubbers [31]. While these studies have generated breakthroughs in terms of overcoming key challenges associated with commercial wearable electronics including rigidity and brittleness, most of them are primarily centered around tuning the materials and not the sensor configuration [31].

Furthermore, wearable sensors are subjected to different kinds of strain due to daily human activities. For instance, in the event of walking, due to the stretching and contraction of joints, a wearable sensor would experience a strain of up to ~55%, which exceeds the limits (~6.5%) for conventional chemical vapor deposition grown graphene (a widely used material in flexible electronics). It is highly desirable for any wearable sensor to have a consistent output and sensitivity under any mechanical deformations owing to human movements. In order to impart stretchability and bendability to the sensor with minimal variance in the resulting electrical signal, previous techniques utilized flexible elastomeric substrates, serpentine electrode design, or multi-layered nanomaterials. However, these devices still suffer from strain dependency due to the presence of structural failure modes. Hence, it is important to design the sensor in a way that will ensure desired response after decoupling signal variations induced by different mechanical deformations [31].

Kirigami is a form of Japanese art, that mainly includes cutting papers and has introduced a new era of flexible, wearable, and deformable structures. These structures have superior stretchability and repeatability due to out-of-plane deformations and thus experience less strain within the structure as compared to the applied strain. High stretchability, repeatability and stability are desired features of wearable sensors that monitor physiological parameters including body temperature and sweat [31].

Here, we report strain-insensitive, flexible temperature and pH sensors on a mesh structured kirigami framework. The major contributions of this part of the thesis work are as follows:

- Detection and real-time monitoring of pH and temperature levels of human body
- Cost-effective roll to roll production on flexible substrates
- High-precision sensitivity and strain-insensitive response under flexion, extension, stretching, and twisting

4.2 Device Fabrication

Our device was designed with a kirigami structure consisting of pH and temperature sensors (Fig. 8). The sensors were printed on a 125 μm thick flexible polymer sheet using the screen-printing method.

Fig. 8. Kirigami shaped Sweat pH and Skin Temperature Sensors

4.3 Kirigami Structure

The kirigami structure of the sensor was laid out surrounding the sensors. The four kirigami arms were spread in such a way that they redistributed the applied strain concentrations symmetrically away from the pH and temperature sensors via the kirigami notches and holes motif. Each of the four arms of the kirigami structure was 1 cm in length and was screen-printed with graphene ink [31].

4.4 pH Sensor

The pH sensor had a two-electrode configuration consisting of circular shaped working electrode (WE) and reference electrode (RE), each having a diameter of 2 mm. Unlike other pH sensors which work on the mechanism of open circuit voltage, our pH sensor is conductive in nature, more specifically resistive. To achieve this circuit characteristics, the Ag/AgCl paste and graphene ink were printed onto the polymer substrate to fabricate the RE and WE, respectively. Afterwards, the WE of the pH sensor was functionalized for pH detection [31].

Polyaniline (PANI) nanofiber arrays were deposited onto the surface of graphene electrode to make the pH sensor highly sensitive to H_3O^+ ions. The redox equilibrium between the phase transitions of H_3O^+ and PANI is suitable for pH sensing. The PANI nanofibers also provide a high surface area, biocompatible, and reproducible performance. PANI layer was electrodeposited on the WE, as shown in Fig. 9.

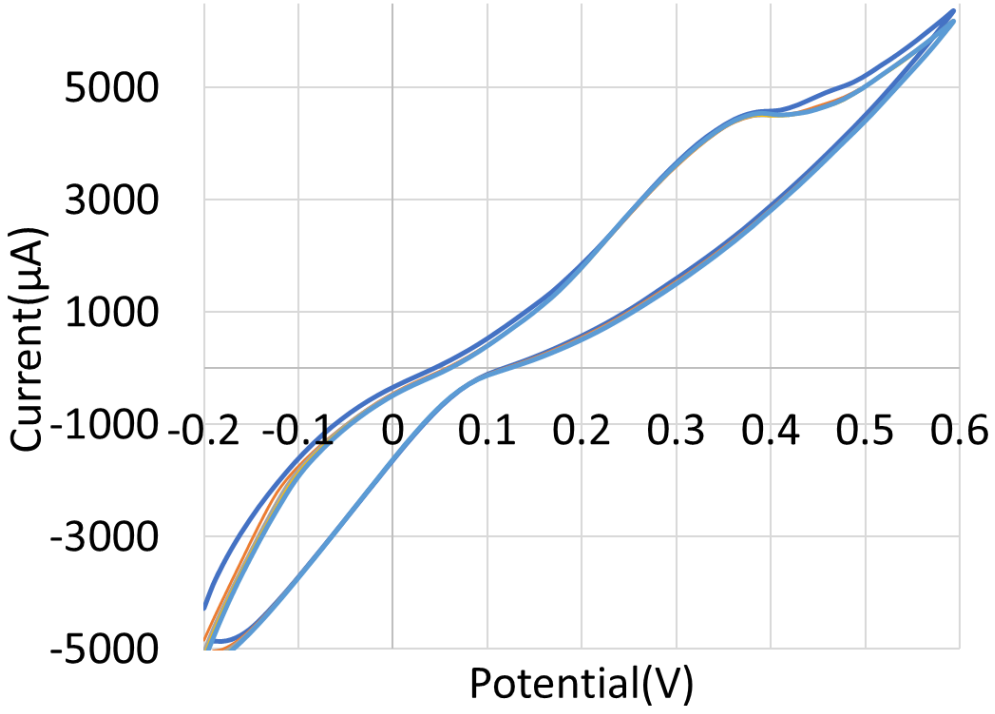

Fig. 9: Cyclic Voltammetry (CV) responses for PANI deposition

4.5 Temperature Sensor

The temperature sensor was prepared by mixing 10mg of PEDOT:PSS with 5mg trion X-100 solution. After sonicating the solution for 10 minutes, (3-glycidyloxypropyl) trimethoxysilane (GOPS) was added with the mixture at 9:1 weight ratio. Then the resulting mixture was sonicated for 10 minutes. At room temperature (25°C), the solution was drop casted onto graphene electrode. The sensor was annealed at 150°C for 1 hour and then cooled in open air for 30 minutes. After that a Kapton tape was added over the sensor [31].

The temperature sensor response was resistive in nature as well [31]. The temperature value was validated by using an LM 35 temperature sensor and then the corresponding resistance value was recorded at each temperature.

4.6 Sensor Characterization

The resistance values of both pH and the temperature sensors were measured with a series resistance topology. As the normal human skin pH is 5.5 and temperature is 35°C, we have calibrated our sensor for pH value from 2 to 13 while the temperature sensor from 25°C to 65°C. The calibration curves for both pH and temperature sensors are shown in Fig.10

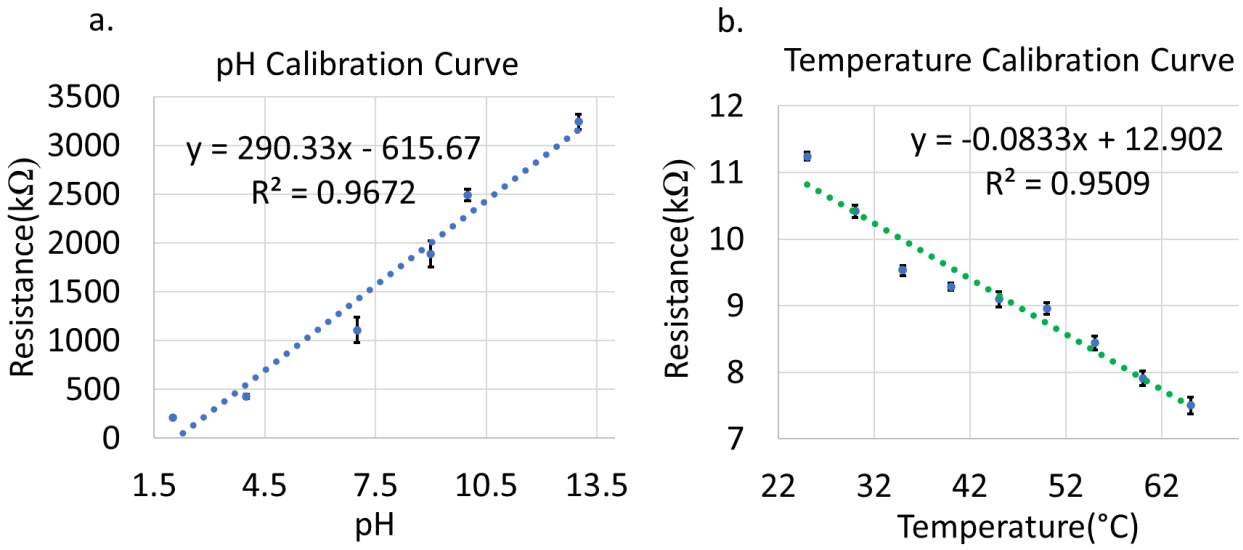

Fig. 10: (a) Calibration plot for pH sensor (from pH 2 to pH 13); (b) Calibration plot for temperature sensor (from 25°C to 65°C)

4.7 Strain-insensitive Characterization

The developed sensor is tested under different flexibility conditions. The four arms of the sensor are stretched simultaneously for validation. The two opposite arms of the sensor are stretched such a way that 220% strain is applied on both sides. Afterwards, the resistance values of pH and temperature sensors are calculated. It has been found that the relative resistance deviation (%ΔR/Ro) of both the pH and temperature sensors is almost the same. The deviation level for temperature sensor is 0.32% while the pH sensor shows a deviation of 0.58%. At 22°C and 48%RH (normal room condition), the resistance response variation of both pH and temperature sensors was verified. The device under different motions of arm is depicted in Fig. 11. The kirigami sensor was also tested for 180° and 360° twisting (Fig. 12a and 12b). The twist test data is shown in Table 2.

Table 2. Kirigami Sensor Flexibility Test

Twist Angle (°)	**pH Sensor Resistance Variation**	**Temperature Sensor Resistance Variation**
180	2.23%	3.58%
360	3.56%	4.53%

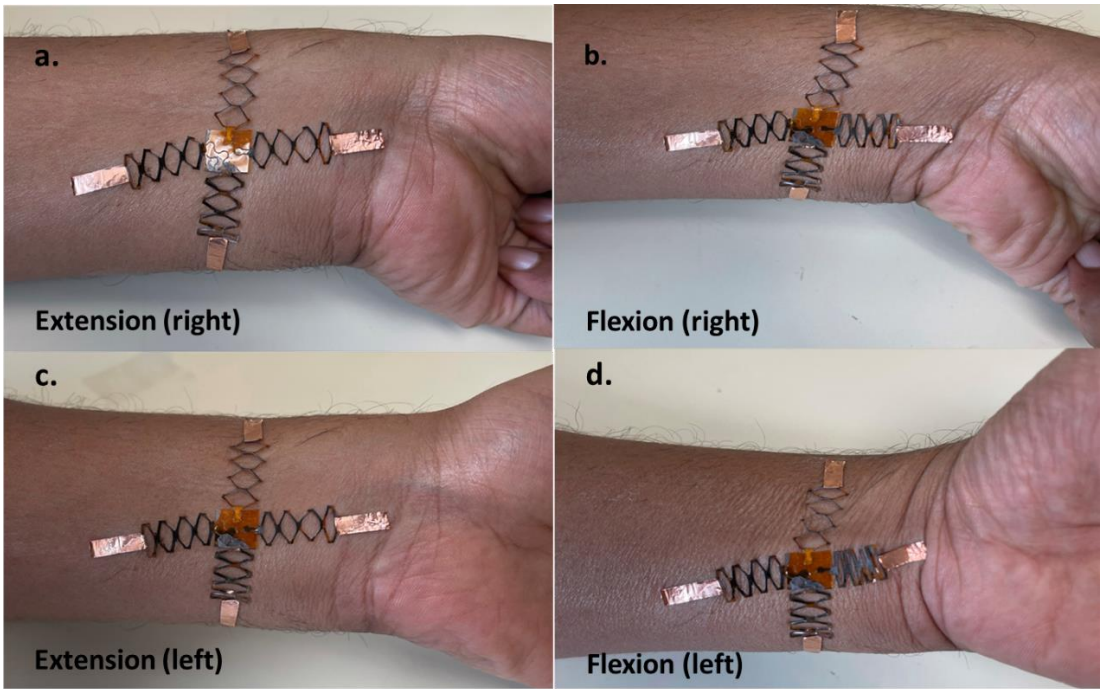

Fig. 11: Kirigami Sensor on human skin. (a) Extension on right side of the hand (b) Flexion on the right; (c) Extension on the left side of the hand; (d) Flexion on the left

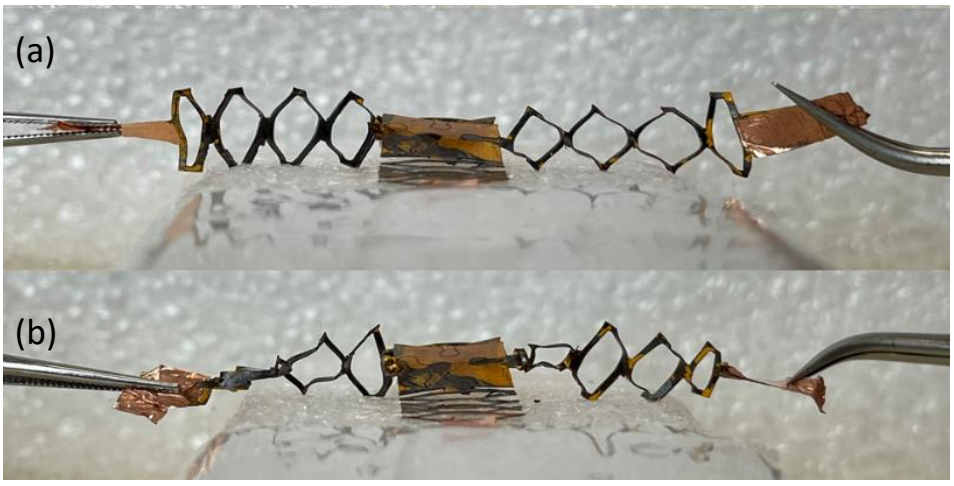

Fig. 12: Kirigami Sensor tested under (a) 180° twisting; (b) 360° twisting

4.8 Summary

In this study, a kirigami-inspired pH and temperature sensors were developed for achieving highly stretchable and strain-insensitive performance in healthcare monitoring. In future, our fully integrated wireless and wearable device has the potential to highlight the sensing platform across a broad range of healthcare applications by enabling personalized care in real-time. Strain-insensitive wearable sensors have aroused substantial attention due to their high precision irrespective of body movements, such as stretching and twisting. This work reports a strain-insensitive pH and temperature sensors based on kirigami structure to quantitively measure and monitor the pH levels in sweat and detect body temperature. Notably, an impressive strain-invariant response was achieved under 220% of applied tensile strain and a torsion up to 360°. By depicting an excellent combination of cost-effectiveness, flexible kirigami structure, breathable notches, high linearity of response, and conformity to skin, our device will open a promising new route in the application of skin-inspired wearable sensors.

Chapter Five

Wound Patch for Real-time Monitoring of Wound Status

5.1 Literature Survey

Based on the origination condition and rate of healing, wounds can be characterized into two major categories, i.e., acute and chronic wounds (which fails to proceed through the normal phase of healing) [32, 33]. For instance, diabetic foot ulcer (DFU) is one kind of severe chronic wound resulting in lower limb amputations in nearly 12% of patients. The global prevalence of diabetes is anticipated to increase from 8.8. to 9.9% by 2045, thereby substantially increasing the risk of DFU development [34, 35]. Although there is no comprehensive data on wound infection, several countries have statistics to estimate the severity of chronic wounds. In Europe, almost 1.5-2 million people are suffering from chronic wounds, and in the US, it is more than 6.5 million causing a serious economic burden on the healthcare treatment that costs up to 25 billion USD per year [36, 37]. Furthermore, with the increase in obesity and diabetes in the elderly population, the number of patients with chronic wounds is increasing exponentially among aged people.

However, to date, real-time immune regulation of skin wound healing is heavily unexplored. The immune cells secrete a cascade of signaling molecules (known as

inflammatory mediators) such as tumor necrosis factor-α (TNF- α), Interleukin-6 (IL-6), Interleukin-8 (IL-8), and Interleukin-10 (IL-10). A delicate balance in the activation of the cytokines, chemokines, and growth factors is crucial to successful wound healing [38, 39].

The anti-inflammatory cytokines function primarily to mediate or suppress the inflammation. The right balance between the pro-and anti-inflammatory responses is crucial to the orderly and timely healing of wounds [40-42]. The wearable wound patch reported in this work (Fig. 13) can provide an accurate, non-invasive, real-time, and continuous monitoring of the dynamics of chronic wounds by real-time tracking of IL-6 and IL-10 levels at the wound site [43].

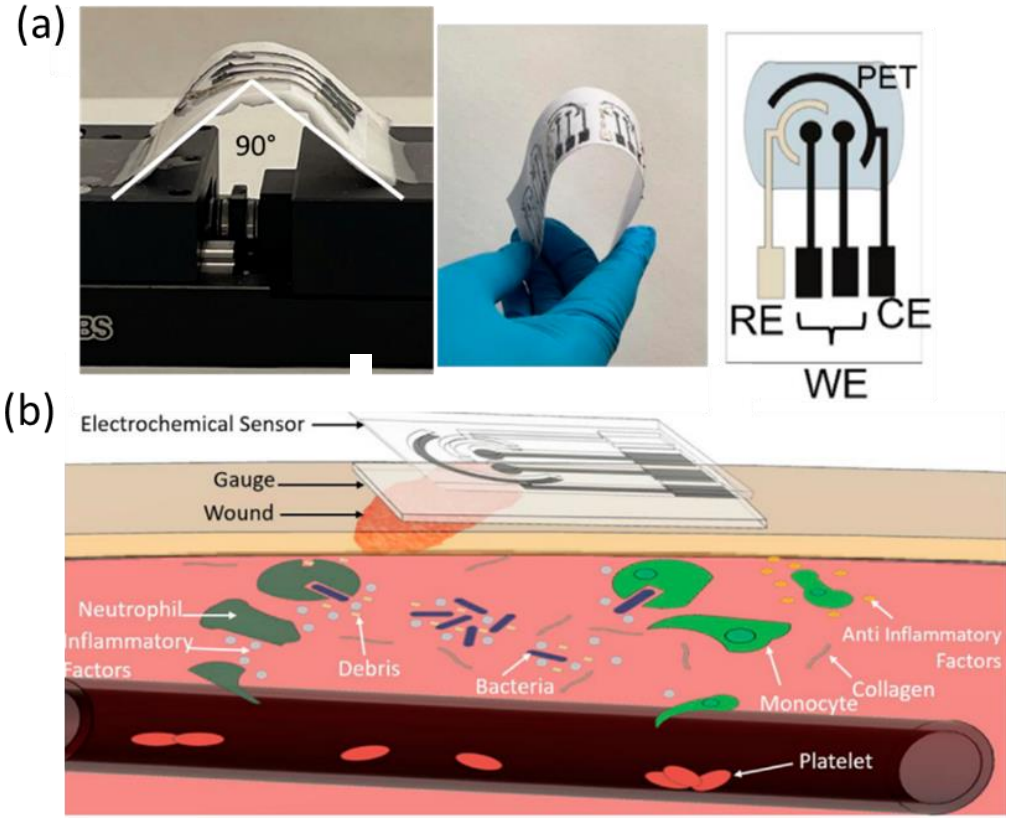

Fig. 13: (a) Experimental Setup of the sensor performance for different degrees of bending (b) Schematic illustration of the wound sensor placed on the wound site for multiplexed detection and monitoring of wound biomarkers

5.2 Electrochemical Characterization

To perform the electrochemical characterization, the Cyclic Voltammetry (CV) in the potential range of –0.2 to +2V at 50mv/s scan rate was conducted using simulated wound fluid (7.4pH). An illustration of CV plots for different functionalized coatings over the working electrode is shown in Fig. 14a. The bare sensor has the least current. The addition of AuNP-MWNT causes the increase of electrostatic interaction owing to the increase of electroactive area as well as the introduction of gold nanoparticles. This modification of the electrode ultimately causes a significant increase in the current with respect to the bare electrode. However, as the linker acid, antibody, and BSA coating are introduced, the CV peak current decreases significantly. The reason for the current decline is the insulating property of the coatings, causing the electron transfer to slow down [43]. The CV plots with and without the AuNP-MWCNT coating is depicted in Fig. 14b. Next, the effect of different scan rate is analyzed. The sweeping of potential from -0.2V to +2V is carried out for different scan rates (Fig 14c).

Finally, to investigate the response time of the sensor, Chronoamperometry (CA) test is carried out so that the characterization of kinetics of chemical reaction can be done. The CA is employed for the sensor with AuNP-MWCNT as well as the sensor without AuNP-

MWCNT by applying a fixed potential of 0.5V across the working and reference electrodes (Fig. 14d).

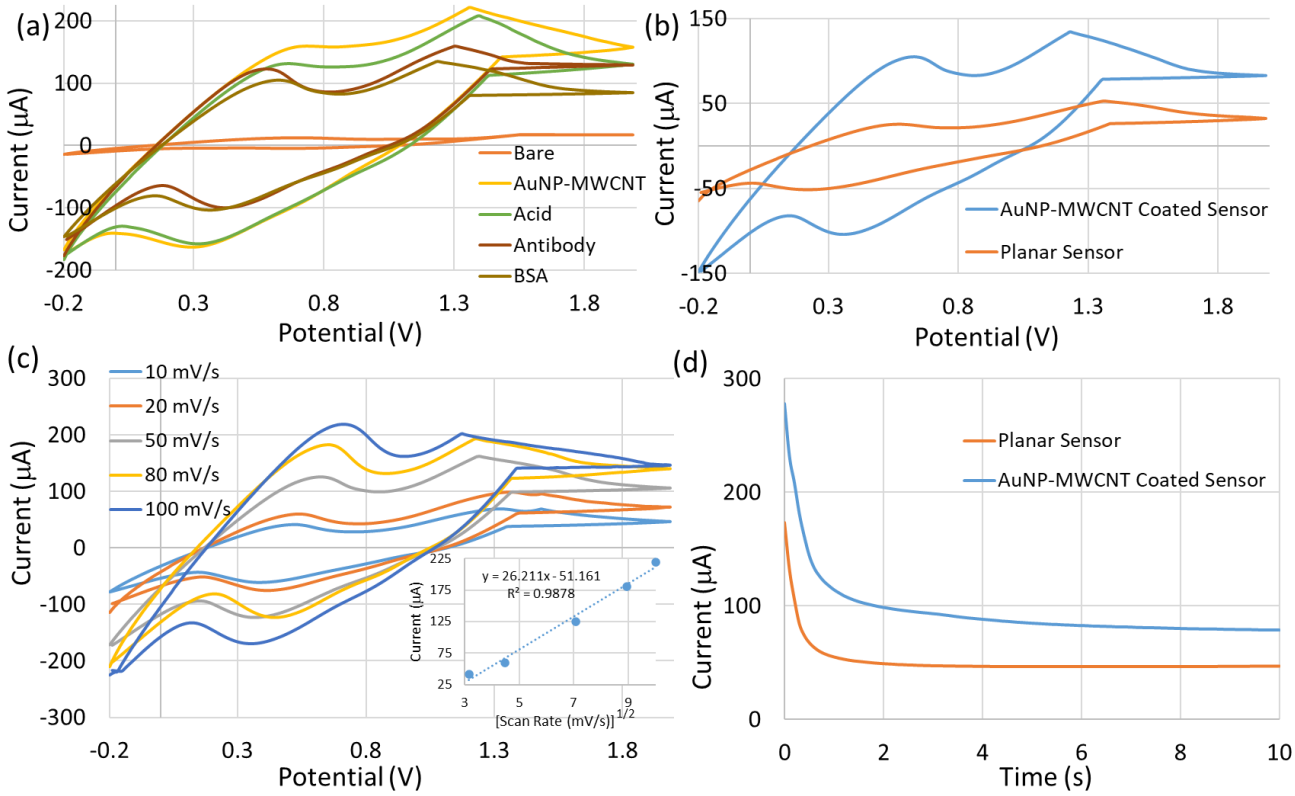

Fig. 14: a) Cyclic Voltammetry curves for different coatings on the WE surface. (b) CV for sensors with and without AuNP-MWCNT coating. (c) CV as a function of scan rate with calibration plot indicating the diffusion-limited behavior of the sensor in the inset. (d) Chronoamperometry plots for sensors with and without AuNP-MWCNT coating

5.3 IL-6 and IL-10 Characterization

For the electrochemical measurements of IL-6 and IL-10, eight different concentrations of each protein biomarker were prepared in Stimulated Wound Fluid (7.4pH). The CV responses for eight different concentrations of IL-6 and IL-10 ranging from 0.1 pg/mL to 1000 pg/mL are depicted in Fig. 15a and Fig. 15b respectively. As the protein concentration is increasing, the redox current is decreasing due to the formation of a thicker immunocomplex insulating layer via binding of a larger number of protein molecules with the antibody-coated sensor surface [43].

The calibration plot for IL-10 with different concentrations of AuNP-MWCNT as well as the planar sensor are shown in Fig. 15c and the calibration curves of IL-6 sensor with and without the AuNP-MWCNT coating are depicted in Fig. 15d.

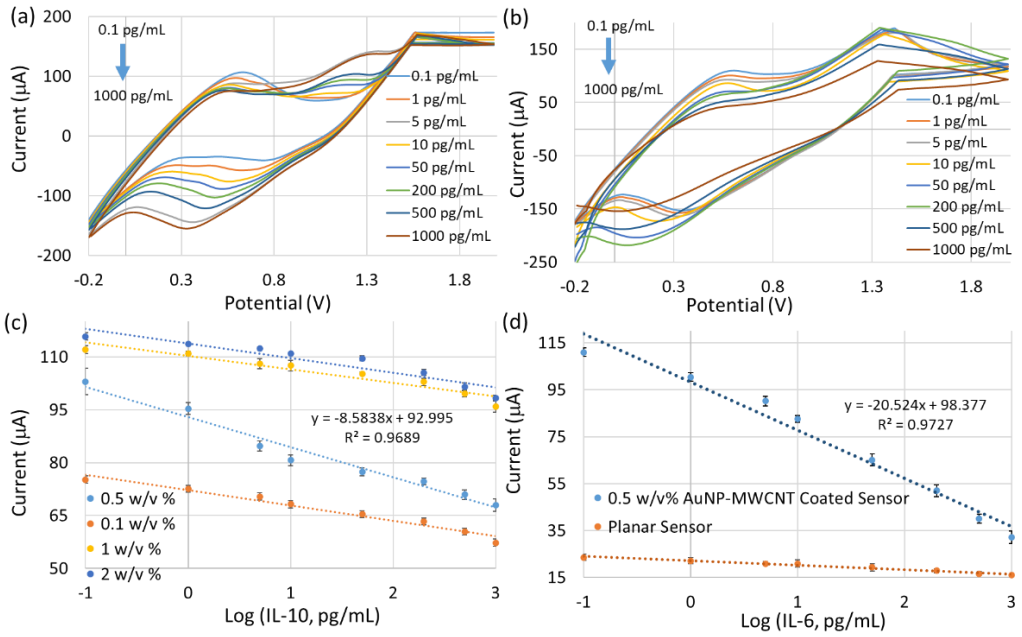

Fig 15: CV plots of 0.5% (w/v) AuNP-MWCNT coated sensor for different concentrations of (a) IL-10 and (b) IL-6. (c) Calibration plots for four different AuNP-MWCNT coatings. (d) Performance comparison between calibration plots of IL-6 sensors with and without the AuNP-MWCNT coating.

5.4 Drift Analysis

The drift of the sensor is analyzed using three concentrations, 0.1 pg/mL, 50 pg/mL, and 1000 pg/mL, of IL- 10, every hour up to 12 hours (Fig. 16a). The sensor was stored at 4°C temperature after each test session. Although the sensor response fluctuates more for the higher concentration as compared to the lower concentration, the relative deviation is less than 5% indicating the minimal drift of the sensor. The drift characteristics of the sensor were also analyzed in 5 minutes time intervals for the three concentrations over 1 hour (Fig. 16b). However, in this case, 0.03% relative deviation indicates significantly less drift characteristics of the sensor in a shorter time interval.

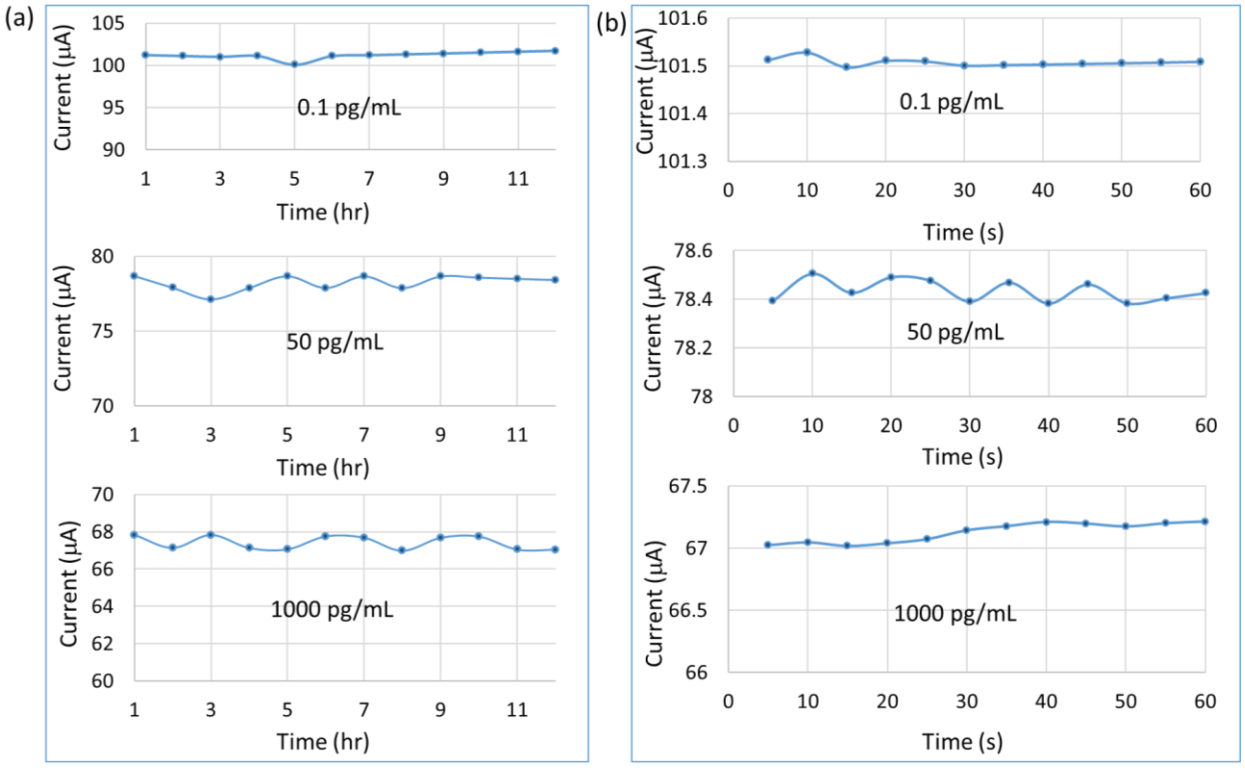

Fig. 16: Drift characteristics of the sensor for three different IL-10 concentrations over (a) 12 h and (b) 1 h.

5.5 Selectivity Analysis

To investigate the sensor's performance in a real chronic wound, a selectivity test is performed (Fig. 17a and Fig 17b). In this test, the sensor was tested with common interferent species such as glucose (180 g/L), cortisol (100 ng/mL), and C-reactive protein (10 pg/mL). The sensor was evaluated with three SWF: first, when there is only interferents present, second, when in addition to the interferents, 10 pg/mL of IL-10 (or IL-6 for IL-6 selectivity) was present, and third, when in addition to interferents 500pg/mL of IL-10 (or

IL-6) was present. The baseline current was nearly identical to the response with interferents. However, the introduction of IL-10 and IL-6 contributes to significant reduction in the oxidation peak current i.e., the increase in difference current with respect to the baseline current.

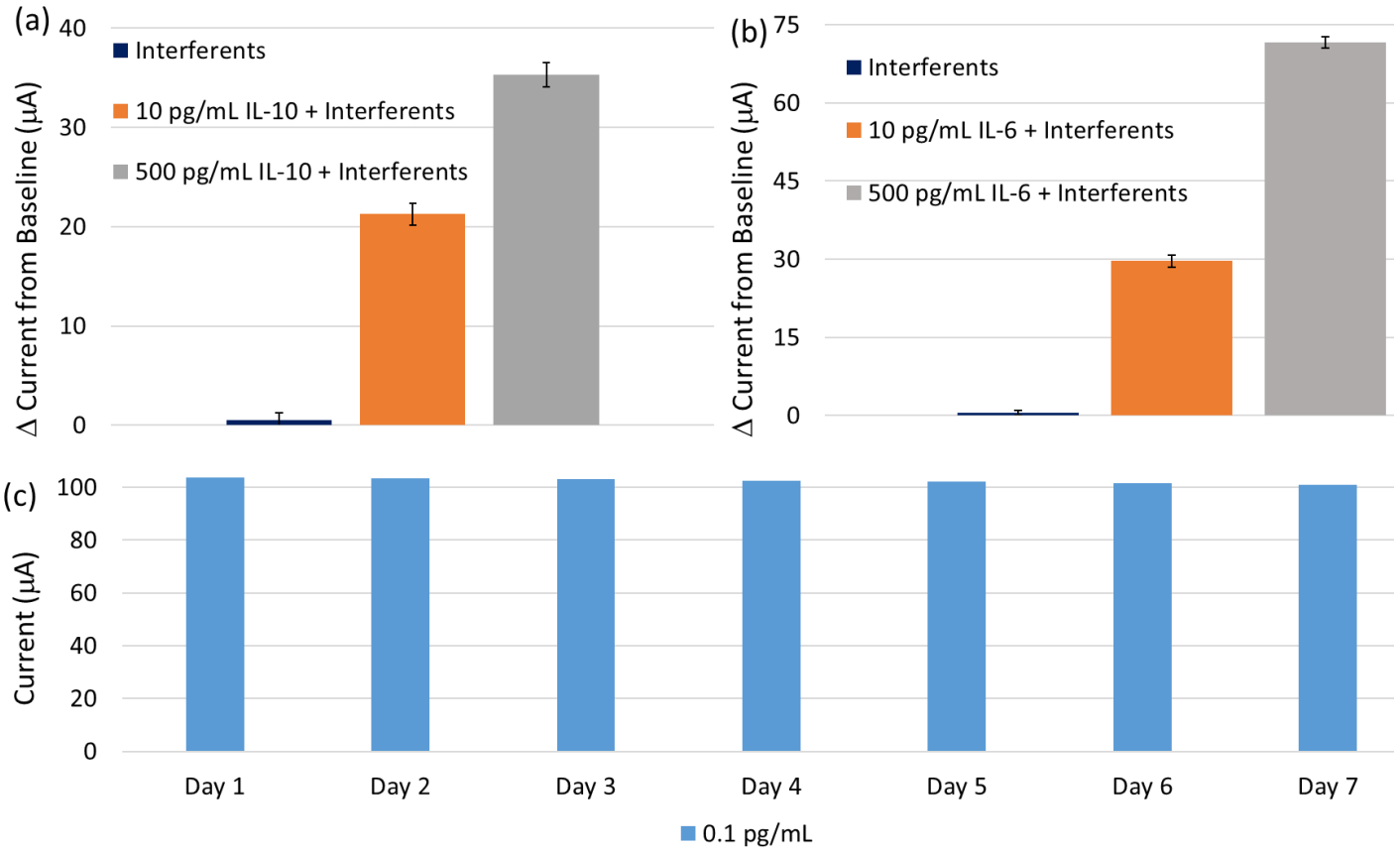

Fig. 17: Selectivity characteristics of the (a) IL-10 and (b) IL-6 sensors in presence of interfering species found in the wound fluids. (c) Lifetime analysis of the sensor over 7 days.

5.6 Lifetime Analysis

To evaluate the lifetime of the sensor, one same sensor was tested with a single concentration for 7 days. At the end of every test, the sensor was stored at 4°C in the fridge. The test results are shown in Fig. 17c

5.7 Summary

In this work, a wearable multiplexed wound patch was developed for monitoring of wound biomarkers in real-time. The complete characterization of sensitivity, selectivity, limit of detection, bending, reproducibility, reversibility, repeatability, and drift analysis were performed. Excellent performance of the wound patch in all the tests proves its potential for on-body measurements enabled with on-demand drug release at the wound site.

Chapter Six

Electrically Controlled Drug Delivery

6.1 Drug Delivery Characterization

The drug delivery component was comprised of two electrodes (Fig. 18a), a reference and a working electrode. After the fabrication of screen-printed drug electrodes on a flexible substrate, the electrodes were functionalized, and a specific drug was loaded on the working electrode using electro co-deposition method [44]. Different known concentrations of drug were prepared to produce the calibration plot. After that, the drug release from two patches were recorded, one without any applied potential and another with a negative applied potential of -0.5V. The released drug was collected at specific time points to quantify the concentrations of the drug. The quantification of released drug was performed with high performance liquid chromatography (HPLC). The drug release rate with an applied potential was much higher than the naturally released rate of drug as shown in Fig. 19b.

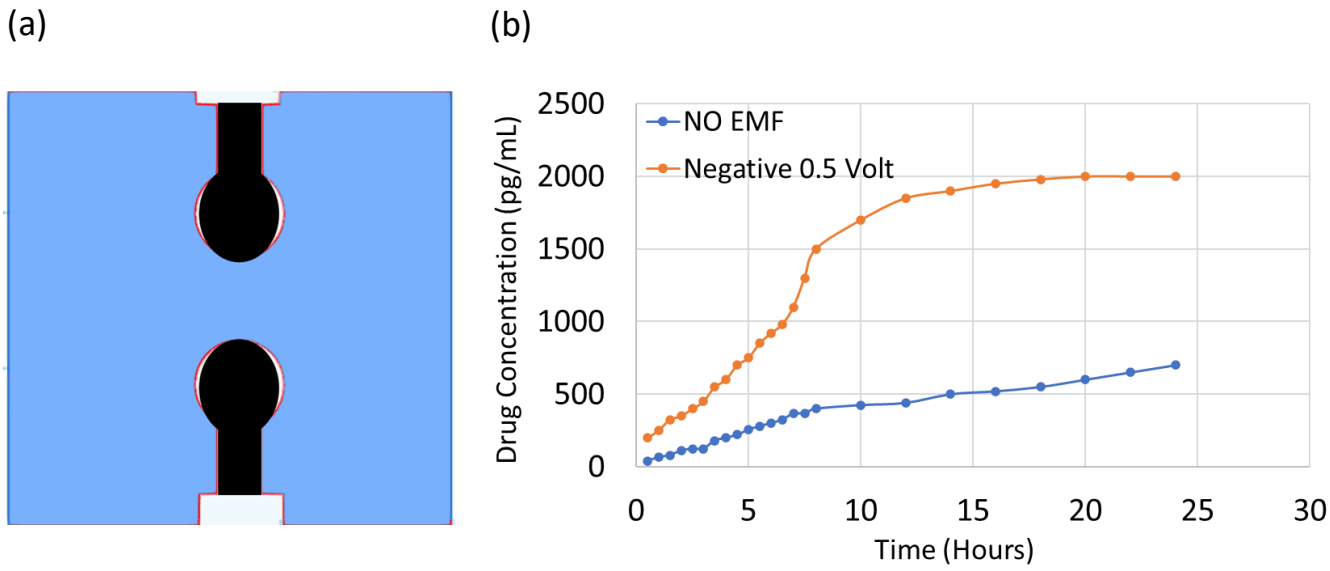

Fig. 18: (a) Design of the drug delivery module. (b) The increased drug release rate under voltage stimulation and decreased natural release without a voltage stimulation.

Chapter Seven

Fully Skin Conformal Tattoo Sensor

Tattoo Sensor Characterization

The developed tattoo sensor is fully conformal to skin and has the potential to be applied in healthcare applications as a sweat sensor for multiplexed monitoring of inflammatory biomarkers in real-time. In order to show the performance of this sensor, the tattoo sensor was functionalized for relative humidity and temperature sensing. The data presented with this wearable tattoo sensor was collected from real-time on-leaf monitoring of relative humidity (RH), temperature, and vapor-pressure deficit (VPD) in both water-stressed and unstressed plants. This tattoo sensor is flexible and fully conformable to the leaf surface. The electrodes on the sensor were functionalized for continuous determination of VPD at the leaf surface to provide information on plant transpiration. Transpiration cools the plants and affects nutrient uptake, photosynthesis, and the transportation of water within the plant-soil system. Vapor-pressure deficit (VPD) works as the driving force for transpiration in plants, suggesting a strong positive relationship between VPD and transpiration rate. VPD takes into account both temperature and RH at the leaf surface and in the air. VPD can be too low or high for optimum plant growth. High VPD indicates a

dry environment for plant indicating that the plant is water stressed, which means the plant needs more water. Drought stress occurs when the transpiration rate calculated from VPD exceeds the rate at which water can translocate from the roots to the plant leaves. In the same way, at low VPD the leaf surface becomes saturated and different plant diseases and fungal growth become the main concerns. In water stressed plants, there is a decrease in the amount of water flowing inside the plant making it difficult for the nutrients to assimilate in the root and then get transported to the other parts of plants. Therefore, continuous monitoring of VPD will aid in controlling plant growth environments and the farmers can take actions earlier to ensure optimum water and nutrient supply, apply disease control measures and improve the production of plants [45]. The experimental set up to collect data from the tattoo sensor is depicted in Fig. 19. The stressed and unstressed plants with tattoo sensors attached on their leaves are depicted in Fig. 20. In addition, the tattoo sensors were attached on the human skin in both relaxed and flexion positions, as shown in Fig. 21.

Fig. 19: Experimental set up with the tattoo sensor

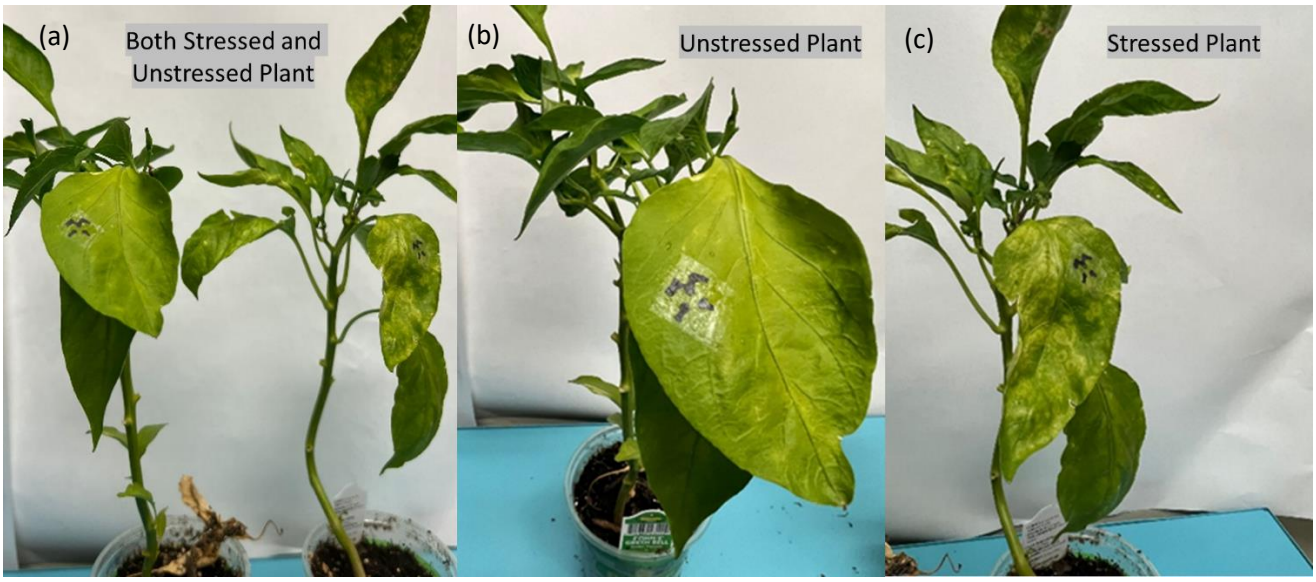

Fig. 20: (a) Plants with tattoo sensors attached to the leaf. Optical images of (b) unstressed and (c) stressed plants

(a) (b)

Fig. 21: Tattoo sensor attached to the human skin at ankle under (a) relaxed and (b) flexion positions

The selective coating for the temperature sensor was composed of gold nanoparticles decorated multiwalled carbon nanotube (AuNP-MWCNT). The humidity sensor was fabricated with functionalized multiwalled carbon nanotube (f-MWCNT) and hydroxyethyl cellulose (HEC) providing an excellent sensitivity to relative humidity variations. The calibration plots for temperature and humidity sensors are given in Fig. 22a and Fig. 22b, respectively.

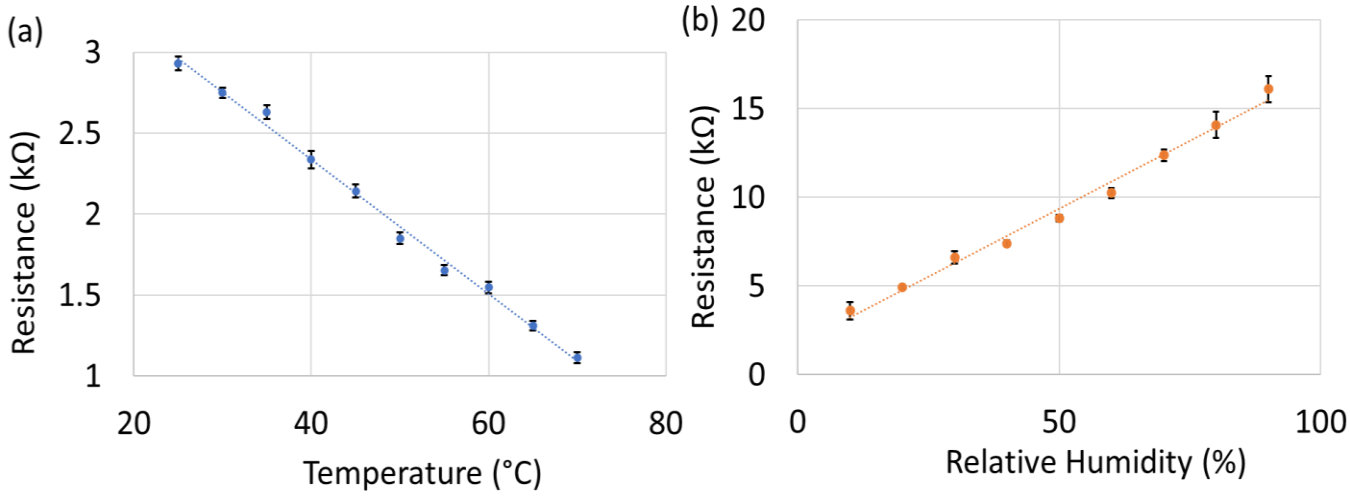

Fig. 22: (a) Calibration curve of temperature sensor. (b) Calibration curve of humidity sensor

Generally, VPD is estimated by

$$VPD = VP_{sat} - VP_{air}.$$

VP_{sat} = saturated vapor pressure at the plant leaf

VP_{air} = air vapor pressure

$$VP_{sat} = 0.6107 \times 10^{7.5\,T_l / (273.3 + T_l)}$$

Where,

T_l = temperature on the leaf in Celsius,

$$VP_{air} = 0.6107 \times 10^{7.5\,T_a / (273.3 + T_a)} \times RH/100$$

Where,

Ta = air temperature in Celsius, and

RH = relative humidity on the leaf surface [45]

After calculating VPD from leaf temperature and RH for both unstressed and stressed plants, it was evident that the VPD for water stressed plant was much higher than the unstressed plant indicating an accurate assessment of plant condition with the tattoo sensor as shown in Fig. 23.

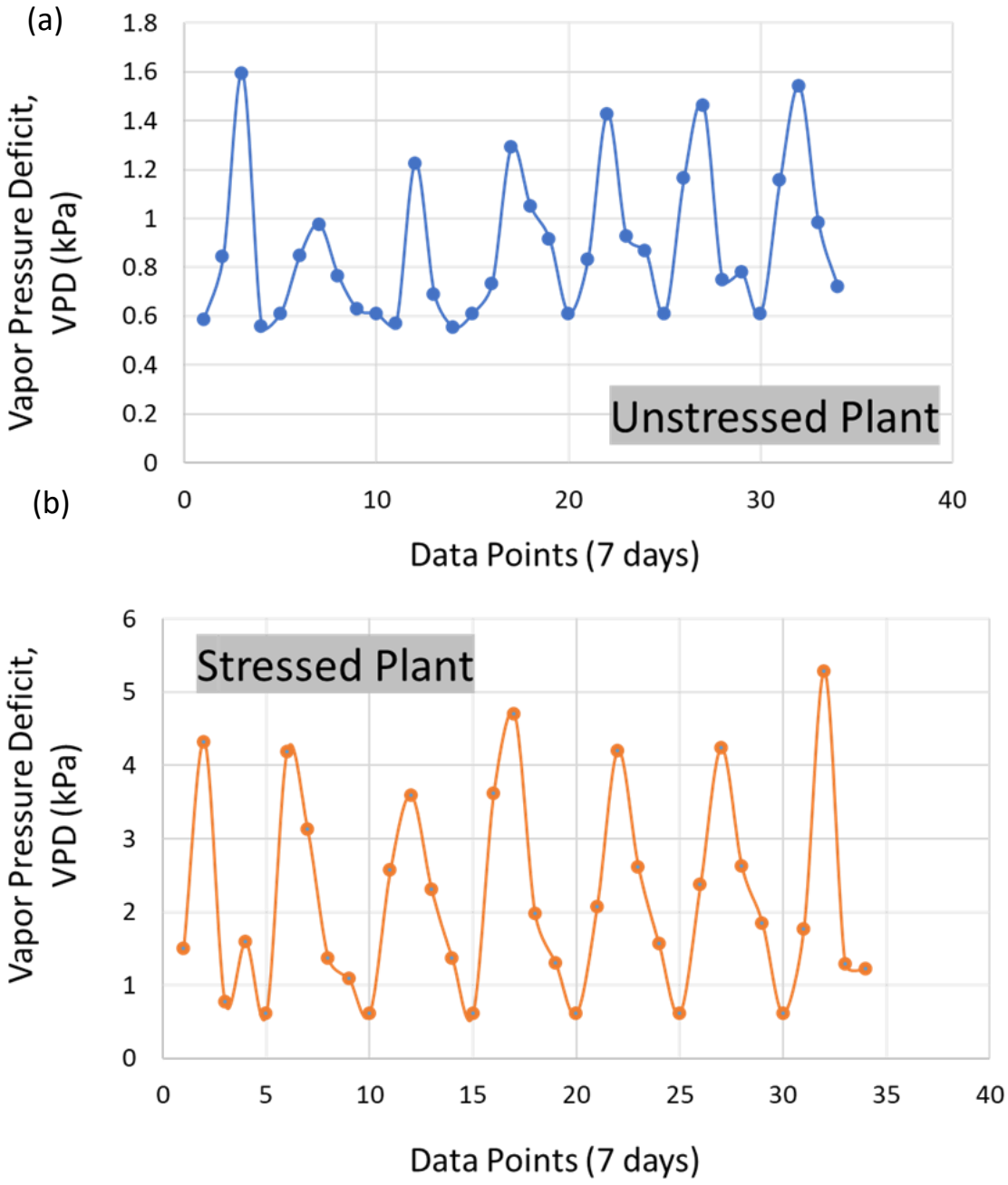

Fig. 23: Vapor Pressure deficit (VPD) in (a) unstressed and (b) stressed plants over 7 days (data was recorded 4 times a day)

Conclusion

In summary, in this thesis work, five different types of flexible wearable sensors were fabricated including, sweat sensor integrated with a microfluidic channel, strain-insensitive kirigami-shaped wearable sensor, wound patch for wound status monitoring from wound fluids, electrically controlled drug delivery unit, and a fully skin conformal tattoo sensor, each focused on a specific application. Different biofunctionalization coatings were synthesized for the detection and monitoring of inflammatory biomarkers. The performance of all the sensors presented in this thesis paper was quite impressive in comparison with recent research reported in the literature. Depending on different substrate materials, functionalization coatings, and targeted molecules and parameters, the sensitivity, LoD, detection range, and reproducibility of different sensors varied. In this thesis work, the highest sensitivity achieved by our sensor for the detection of inflammatory biomarkers was 653.279 $\mu A\ (pg/mL)^{-1}\ cm^{-2}$ for a detection range from 0.1 pg/mL to 1000 pg/mL with an LoD of 9 × 10-3 pg/mL [43]. The sensors also exhibited highly selective and reproducible performance. The lifetime of the sensors was characterized over 7 days, and the sensors exhibited stable response during that one-week period. Further extension of the lifetime can be achieved in the future. In conclusion, the performance of all the sensors were excellent and satisfactory.

References

[1] W. Ansar, and S. Ghosh, "Inflammation and inflammatory diseases, markers, and mediators: role of CRP in some inflammatory diseases," Biology of C Reactive Protein in Health and Disease, pp. 67-107, 2016.

[2] K. H. Allin, B. G. Nordestgaard, H. Flyger H, S. E. Bojesen, "Elevated pretreatment levels of plasma C-reactive protein are associated with poor prognosis after breast cancer: a cohort study," Breast Cancer Res., vol. 13, no. 3, 2011.

[3] P. Salvo, V. Dini, A. Kirchhain, A. Janowska, T. Oranges, A. Chiricozzi, T. Lomonaco, F. Di Francesco, and M. Romanelli, "Sensors and biosensors for C-reactive protein, temperature and pH, and their applications for monitoring wound healing: A Review," Sensors, vol. 17, no. 12, pp. 2952, 2017.

[4] A. S. Cruz, et al., "Interleukin-6 Is a Biomarker for the Development of Fatal Severe Acute Respiratory Syndrome Coronavirus 2 Pneumonia," Frontiers in Immunology, vol. 12, 2021.

[5] Z.-Q. Lin, T. Kondo, Y. Ishida, T. Takayasu, and N. Mukaida, "Essential involvement of IL-6 in the skin wound-healing process as evidenced by delayed wound healing in IL-6-deficient mice," Journal of Leukocyte Biology, vol. 12, no. 6, pp. 713-721, 2003.

[6] L. Lu, H. Zhang, D. J. Dauphars DJ, and Y.-W. He, “A Potential Role of Interleukin 10 in COVID-19 Pathogenesis,” Trends Immunol., vol. 42, no. 1, pp. 3-5, 2021.

[7] I. Hashim, T. C. Chamberlain, A. L. Mui, and J. P. Little, “Elevated Interleukin-10 Levels in COVID-19: Potentiation of Pro-Inflammatory Responses or Impaired Anti-Inflammatory Action,” Frontiers in Immunology, vol. 12, 2021.

[8] M. T. Gonzalez-Garza, D. E. Cruz-Vega, and C. Maldonado-Bernal, "IL10 as Cancer Biomarker", in Translational Research in Cancer. London, United Kingdom: IntechOpen, 2020.

[9] S. A. Eming, S. Werner, P. Bugnon, C. Wickenhauser, L. Siewe, O. Utermöhlen, J. M. Davidson, T. Krieg, and A. Roers, “Accelerated wound closure in mice deficient for interleukin-10. Am J Pathol.” Vol. 170, no. 1, pp. 188-202, Jan 2007.

[10] E. J.M. Moonen, J. R. Haakma, E. Peri, E. Pelssers, M. Mischi, and J. M.J. den Toonder, “Wearable sweat sensing for prolonged, semicontinuous, and nonobtrusive health monitoring,” View, vol. 1, no. 4, December 2020.

[11] Y. Yang, Y. Song, X. Bo, J. Min, O. S. Pak, L. Zhu, M. Wang, J. Tu, A. Kogan, H. Zhang, T. K. Hsiai, Z. Li, and W. Gao, “A laser-engraved wearable sensor for sensitive detection of uric acid and tyrosine in sweat,” Nat Biotechnol., vol. 38, no. 2, pp. 217-224, Feb 2020.

[12] M. Caldara, C. Colleoni, E. Guido, G. Rosace, V. Re and A. Vitali, "A wearable sensor platform to monitor sweat pH and skin temperature," 2013 IEEE International Conference on Body Sensor Networks, pp. 1-6, 2013.

[13] A. E. Kitabchi, G. E. Umpierrez, J. M. Miles, and J. N. Fisher, "Hyperglycemic Crises in Adult Patients With Diabetes," Diabetes Care, vol. 32, no. 7, pp. 1335-1343, 2009.

[14] S. Tharakan, K. Nomoto, S. Miyashita, and K. Ishikawa, "Body temperature correlates with mortality in COVID-19 patients," Critical Care, vol. 24, pp. 298, 2020.

[15] M. Yu, G. Yu and B. Dai, "Graphene Fiber-Based Strain-Insensitive Wearable Temperature Sensor," in IEEE Sensors Letters, vol. 4, no. 10, pp. 1-4, 2020.

[16] M. K. Blees, A. W. Barnard, P. A. Rose, S. P. Roberts, K. L. McGill, P. Y. Huang, A. R. Ruyack, J. W. Kevek, B. Kobrin, D. A. Muller, P. L. McEuen, "Graphene kirigami," Nature, vol. 524, no. 7564, pp. 204-7, 2015.

[17] K. Yong, S. De, E. Y. Hsieh, J. Leem, N. R. Aluru, S.-W. Nam, "Kirigami-inspired strain-insensitive sensors based on atomically-thin materials," Materials Today, vol. 34, no. 4, p. 58-65, 2020.

[18] P. Chansai, A. Sirivat, S. Niamlang, D. Chotpattananont, and K. Viravaidya-Pasuwat, "Controlled transdermal iontophoresis of sulfosalicylic acid from polypyrrole/poly(acrylic acid) hydrogel," International Journal of Pharmaceutics, vol. 381, no. 1, pp. 25–33, 2009.

[19] M. A. Ali, C. Hu, S. Jahan, B. Yuan, M. S. Saleh, E. Ju, S. J. Gao, and R. Panat, "Sensing of COVID-19 antibodies in seconds via aerosol jet nanoprinted reduced-graphene-oxide-coated 3D electrodes," Advanced Materials, vol. 33, no. 7, p. 2006647, 2020.

[20] M. Rezaei, S. Razavi Bazaz, S. Zhand, N. Sayyadi, D. Jin, M. P. Stewart, and M. Ebrahimi Warkiani, "Point of care diagnostics in the age of covid-19," Diagnostics, vol. 11, no. 1, p. 9, 2020.

[21] M. A. Ali, S. Tabassum, Q. Wang, Y. Wang, R. Kumar, and L. Dong, "Integrated dual-modality microfluidic sensor for biomarker detection using lithographic Plasmonic Crystal," Lab on a Chip, vol. 18, no. 5, pp. 803–817, 2018.

[22] J. P. Broughton, X. Deng, G. Yu, C. L. Fasching, V. Servellita, J. Singh, X. Miao, J. A. Streithorst, A. Granados, A. Sotomayor-Gonzalez, K. Zorn, A. Gopez, E. Hsu, W. Gu, S. Miller, C.-Y. Pan, H. Guevara, D. A. Wadford, J. S. Chen, and C. Y. Chiu, "CRISPR–CAS12-based detection of SARS-COV-2," Nature Biotechnology, vol. 38, no. 7, pp. 870–874, 2020.

[23] N. Zhu, D. Zhang, W. Wang, X. Li, B. Yang, J. Song, X. Zhao, B. Huang, W. Shi, R. Lu, P. Niu, F. Zhan, X. Ma, D. Wang, W. Xu, G. Wu, G. F. Gao, and W. Tan, "A novel coronavirus from patients with pneumonia in China, 2019," New England Journal of Medicine, vol. 382, no. 8, pp. 727–733, 2020.

[24] V. M. Corman, O. Landt, M. Kaiser, R. Molenkamp, A. Meijer, D. K. W. Chu, T. Bleicker, S. Brünink, J. Schneider, M. L. Schmidt, D. G. J. C. Mulders, B. L. Haagmans, B. van der Veer, S. van den Brink, L. Wijsman, G. Goderski, J.-L. Romette, J. Ellis, M. Zambon, M. Peiris, H. Goossens, C. Reusken, M. P. G. Koopmans, and C. Drosten, "Detection of 2019 novel coronavirus (2019-ncov) by real-time RT-PCR," Eurosurveillance, vol. 25, no. 3, 2020.

[25] T. Wen, C. Huang, F.-J. Shi, X.-Y. Zeng, T. Lu, S.-N. Ding, and Y.-J. Jiao, "Development of a lateral flow immunoassay strip for rapid detection of IGG antibody against SARS-COV-2 virus," The Analyst, vol. 145, no. 15, pp. 5345–5352, 2020.

[26] A. Powers and S. Palecek, "Protein analytical assays for diagnosing, monitoring, and choosing treatment for cancer patients," Journal of Healthcare Engineering, vol. 3, no. 4, pp. 503–534, 2012.

[27] A. S. Gauchez, N. Ravanel, D. Villemain, F. X. Brand, D. Pasquier, R. Payan and M. Mousseau, “Evaluation of a manual ELISA kit for determination of HER2/neu in serum of breast cancer patients”, Anticancer Res., vol. 28, pp. 3067–3073, 2008.

[28] J.-R. Lavillegrand, M. Garnier, A. Spaeth, N. Mario, G. Hariri, A. Pilon, E. Berti, F. Fieux, S. Thietart, T. Urbina, M. Turpin, L. Darrivere, M. Fartoukh, F. Verdonk, G. Dumas, A. Tedgui, B. Guidet, E. Maury, Y. Chantran, G. Voiriot, and H. Ait-Oufella, “Elevated plasma IL-6 and CRP levels are associated with adverse clinical outcomes and death in critically ill SARS-COV-2 patients: Inflammatory response of SARS-COV-2 patients,” Annals of Intensive Care, vol. 11, no. 1, 2021.

[29] T. Noushin and S. Tabassum, "Multiplexed Electrochemical Sensor for Real-Time Monitoring of Inflammatory Biomarkers," 2021 IEEE Sensors, 2021, pp. 1-4, doi: 10.1109/SENSORS47087.2021.9639859.

[30] T. Noushin and S. Tabassum, “WRRIST: A wearable, rapid, and real-time infection screening tool for dual-mode detection of inflammatory biomarkers in sweat,” Microfluidics, BioMEMS, and Medical Microsystems XX, 2022.

[31] T. Noushin, N. I. Hossain, and S. Tabassum, “Kirigami-patterned highly stable and strain insensitive sweat ph and temperature sensors for long-term wearable applications,” 2022 IEEE Healthcare Innovations and Point of Care Technologies (HI-POCT), 2022.

[32] C. K. Sen, G. M. Gordillo, S. Roy, R. Kirsner, L. Lambert, T. K. Hunt, F. Gottrup, G. C. Gurtner, and M. T. Longaker, "Human skin wounds: A major and snowballing threat to public health and the economy," Wound Repair and Regeneration, vol. 17, no. 6, pp. 763–771, 2009.

[33] M. Farahani and A. Shafiee, "Wound healing: From passive to smart dressings," Advanced Healthcare Materials, vol. 10, no. 16, p. 2100477, 2021.

[34] E. Standl, K. Khunti, T. B. Hansen, and O. Schnell, "The global epidemics of diabetes in the 21st century: Current situation and perspectives," European Journal of Preventive Cardiology, vol. 26, no. 2_suppl, pp. 7–14, 2019.

[35] W. Clayton and T. A. Elasy, "A review of the pathophysiology, classification, and treatment of foot ulcers in diabetic patients," Clinical Diabetes, vol. 27, no. 2, pp. 52–58, 2009.

[36] E. Zimlichman, D. Henderson, O. Tamir, C. Franz, P. Song, C. K. Yamin, C. Keohane, C. R. Denham, and D. W. Bates, "Health Care–Associated infections," JAMA Internal Medicine, vol. 173, no. 22, p. 2039, 2013.

[37] C. J. Phillips, I. Humphreys, J. Fletcher, K. Harding, G. Chamberlain, and S. Macey, "Estimating the costs associated with the management of patients with chronic wounds using linked routine data," International Wound Journal, vol. 13, no. 6, pp. 1193–1197, 2015.

[38] A. McLister, J. Phair, J. Cundell, and J, Davis, "Electrochemical approaches to the development of smart bandages: A mini-review," Electrochem. Commun., vol. 40, pp. 96–99, 2014.

[39] A. McLister, A. Mathur, and J. Davis, "Wound diagnostics: Deploying electroanalytical strategies for point of care sensors and smart dressings," Current Opinion in Electrochemistry, vol. 3, no. 1, pp. 40–45, 2017.

[40] M. L. Novak and T. J. Koh, "Macrophage phenotypes during tissue repair," Journal of Leukocyte Biology, vol. 93, no. 6, pp. 875–881, 2013.

[41] A. Mantovani, S. K. Biswas, M. R. Galdiero, A. Sica, and M. Locati, "Macrophage plasticity and polarization in tissue repair and remodelling," The Journal of Pathology, vol. 229, no. 2, pp. 176–185, 2013.

[42] S. Kundu, S. Tabassum, and R. Kumar, "A perspective on sepsis pathogenesis, biomarkers and diagnosis: A concise survey," MEDICAL DEVICES & SENSORS, vol. 3, no. 4, 2020.

[43] T. Noushin, N. I. Hossain, and S. Tabassum, "IOT-enabled integrated smart wound sensor for multiplexed monitoring of inflammatory biomarkers at the wound site," Frontiers in Nanotechnology, vol. 4, 2022.

[44] G. Xu, Y. Lu, C. Cheng, X. Li, J. Xu, Z. Liu, J. Liu, G. Liu, Z. Shi, Z. Chen, F. Zhang, Y. Jia, D. Xu, W. Yuan, Z. Cui, S. S. Low, and Q. Liu, "Battery-free and wireless smart wound dressing for wound infection monitoring and electrically controlled on-demand drug delivery," Advanced Functional Materials, vol. 31, no. 26, p. 2100852, 2021.

[45] S. Yin, H. Ibrahim, P. S. Schnable, M. J. Castellano, and L. Dong, "A field-deployable, Wearable Leaf sensor for continuous monitoring of vapor-pressure deficit," Advanced Materials Technologies, vol. 6, no. 6, p. 2001246, 2021.

Appendix

AS – Artificial Sweat

AuNP - Gold nanoparticles

AuNP-MWCNT - Gold nanoparticles decorated multi-walled carbon nanotube

BSA - Bovine serum albumin

CA – Chronoamperometry

CE - Counter electrode

CLIA - Chemiluminescence immunoassay

CNT - Carbon nanotube

CRISPR - Clustered regularly interspaced short palindromic repeats

CRP - C-reactive Protein

CV - Cyclic Voltammetry

DFU - Diabetic foot ulcer

EDC - Ethylene dichloride

ELISA - Enzyme-linked immunosorbent assay

f-MWCNT - Functionalized multiwalled carbon nanotube

GOPS - 3-glycidyloxypropyl trimethoxysilane

HEC - Hydroxyethyl cellulose

HPLC - High performance liquid chromatography

IL-6 - Interlukin-6

IL-10 - Interlukin-10

IL-8 - Interleukin-8

LFIA - Lateral flow immunoassay

LoD - Limit-of-detection

NHS – N-hydroxysuccinimide

PANI – Polyaniline

PBS - Phosphate buffered saline

PCT – Procalcitonin

PEDOT:PSS - Poly(3,4-ethylenedioxythiophene)-poly(styrenesulfonate)

RE - Reference electrode

RH - Relative humidity

RT-qPCR - Reverse transcription real-time quantitative polymerase chain reaction

TNF- α - Tumor necrosis factor-α

VPD - Vapor-pressure deficit

WE - Working electrode